GLUCAN SYNTHASE-LIKE5 promotes anther callose deposition to maintain timely initiation and progression of meiosis in rice (*Oryza sativa* L.)

Harsha Somashekar

Doctor of Philosophy

Department of Genetics, School of Life Science
The Graduate University for Advanced Studies, SOKENDAI

INDEX

Introduction

Meiosis is a special type of eukaryotic cell division in which one round of DNA replication is followed by two consecutive cell divisions to produce four haploid gametes in animals, or spores in land plants (embryophytes). Despite the fact that meiosis is thought to have evolved from mitosis, it differs from mitosis in several ways, such as programmed DNA double strand break (DSB) formation, meiosis-specific chromosome assembly/organization (homolog alignment and synapsis), crossing over formation, and reductional chromosome segregation. As a result, these events complicate and lengthen the meiotic cell cycle process. Although many of the typical meiotic events occur during the prolonged G2 phase, also known as prophase I, the chromatin loading of meiotic proteins/factors occurs concurrently with premeiotic DNA replication, as a requirement for executing meiotic specific events related to recombination and chromosome segregation in all sexually reproducing organisms such as yeasts (Watanabe et al. 1995; Murakami and Keeney, 2014), plants (Higgins et al. 2012) and mammals (Pratto et al. 2021). Thus, studies on the meiosis-specific mode of cell cycle control (hereafter referred to as "meiotic cell-cycle") and related aspects around the premeiotic DNA synthesis phase (S-phase) are important to understand the molecular machinery that drives meiosis initiation and progression.

In flowering plants, successful pollen production involves a series of multiple complicated steps. An important earlier step is meiosis that takes place within the microsporangium or pollen sac, two pairs of which compose an angiosperm anther (Fig. 1A) (Scott et al. 2004; Zhang and Wilson, 2009). In rice anthers, each of four microsporangia comprises central sporogenous cells (SPCs) surrounded by concentric four-layered somatic cell walls viz. tapetum, middle layer, endothecium and epidermis from inside-out respectively, prior to male meiosis onset (Fig. 1B). After several mitotic divisions, SPCs mature into meiotically competent pollen mother cells (PMCs), and undergo meiosis following DNA replication to halve chromosome number and produce microspores which develop into pollen grains that eventually supply male gametes for fertilization. Parallelly, the tapetal cell (TC) layers provide metabolites and nutrients for neighbouring PMCs and microspores, and eventually ends via the programmed cell death (Dickinson and Bell, 1976; Lei and Liu, 2020; Steer, 1977). The molecular mechanisms underlying floral development, central meiotic events such as homolog pairing and crossing over, and post-meiotic gametogenesis have been extensively studied. In contrast, the mechanisms driving the transition from mitosis to meiosis processes in flowering plants have largely remained elusive.

Our group previously reported that MEIOSIS ARRESTED AT LEPTOTENE2 (MEL2), an RNA recognition motif protein, functions in timely transition of spore mother cells, including both PMCs and female megaspore mother cells (MMCs), to the meiotic cycle in rice (Nonomura et al. 2011). Interestingly,

the expression of several key meiotic genes with known and unknown functions were significantly downregulated in premeiotic *mel2* mutant anthers (Mimura et al. 2021). One of the candidate downregulated gene with known function in pollen development but unknown meiotic function was *GLUCAN SYNTHASE-LIKE5* (*OsGSL5*) (Mimura et al. 2021), which is the main player of this study. Among 10 rice *GSL* genes, *OsGSL5* is the only gene expressing preferentially and abundantly in anthers during meiosis and post-meiosis (Yamaguchi et al. 2006; Shi et al. 2015) (Fig. 2). To ascertain that GSL5 is truly under the control of MEL2, I performed reverse transcription quantitative PCR (RT-qPCR) and aniline blue staining that specifically stains callose polymer, in *mel2* mutant anthers. As expected, the GSL5 transcripts levels were significantly downregulated and also callose accumulation was largely eliminated from *mel2* anther locules during premeiosis and meiosis (Figs. 3, 4), confirming that OsGSL5 is involved in the downstream network of the MEL2 cascade. These observations have strongly suggested an unknown association of callose deposition with meiotic entry control in plants. OsGSL5 encodes glucan/callose synthase, one of the enzymes responsible for the biosynthesis of callose, a plant specific polysaccharide.

Callose is made up of linear glucose residues of β-1,3 linkages, with some having β-1,6-glucan branches, and functions in various aspects of plant growth and development spatio-temporally (Stone and Clarke, 1992; Chen and Kim, 2009; Zavaliev et al. 2011; Piršelová and Matušíková, 2013; Nedhuka, 2015). For instance, callose is involved in papillae cell-wall materials at bacterial and fungal contact site (Dong et al. 2008; Voigt, 2014) and also secreted at wounded plant tissues (Jacobs et al. 2003), highlighting the prominent roles of callose in host defense mechanisms against both biotic and abiotic stresses. Callose is also an integral part of the plasmodesmata (PD), cytoplasmic channels/bridges connecting two neighbouring cells in almost all plant organs/ tissues, except in some food and water conducting tissues/cells such as sieve tubes and tracheary elements (Barnett, 1982; Beebe et al. 1992). In cell-cell signaling context in plants, callose regulates the conductivity of PDs and largely influences the diffusion of signals between the cells (Radford et al. 1998; Lucas et al. 2009; Lee and Sieburth, 2010; Zavaliev et al. 2011; Sager and Lee, 2018). In addition to controlling symplastic signaling, callose is also thought to permit direct diffusion of signals on cell walls, as affecting the mechanical/chemical properties of cell walls (apoplastic signaling) (Maltby et al. 1979; Bhalla and Slattery, 1984; Yim and Bradford, 1998; Abou-Saleh et al. 2018). Besides, callose is also deposited transiently at dividing cell plates during cytokinesis, and aids in the formation primary wall between the dividing daughter cells (Staehelin and Heplar, 1996; Hong et al. 2001; Thiele et al. 2009). It is also deposited at phloem tissue to control sieve plate development and pore size of sieve tubes (Xie et al. 2011).

During the transition from mitosis to meiosis in flowering plants, an extensive remodeling of

germ cell walls takes place, whereby the cellulosic-rich PMC walls are drastically rearranged and replaced by callose (Matsuo et al. 2013, also see Fig. 21). Such hyper callose accumulation in anther locules, referred to as "histological hallmark" of PMCs entering meiosis, marks the initiation of meiosis division in sexual plants, while it was enigmatic as to why such drastic turnover (biological meaning) of PMCs wall composition from cellulose to callose is required during mitosis to meiosis transition time. Several reports have revealed the importance of callose accumulation during microsporogensis and megasporogenesis (female reproduction events). In Arabidopsis, *CALLOSE SYNTASE5* (*CalS5*) exerts essential functions during pollen formation stages (Dong et al. 2005). Similarly, the rice *OsGSL5*, a homolog of *AtCalS5*, is responsible for pollen growth and development during microsporogensis (Shi et al. 2015). Premature dissolution of callose in the rice *defective callose in meiosis1 (dcm1)* mutant generates abnormal pollen grains with varied size and DNA content as a result of defects in meiotic cytokinesis (Zhang et al. 2018). Callose also helps in the microspore/pollen growth and development, patterning of pollen aperture and elongation of pollen tubes (Franklin-Tong, 1999; Albert et al. 2011; Qin P et al. 2012; Prieu et al. 2017). In female reproduction, callose is deposited around MMCs prior to meiosis, similar to PMCs, and also surrounds megaspores, where it forms a physical barrier before being degraded in both functional and degenerating megaspore (Tucker & Koltunow, 2014; Bachelier, J.B., & Friedman, W.E. 2011). In contrast, little is known about the roles of hyper callose accumulation in premeiotic anther development and male meiosis, despite of its noticeable amounts and cross-species conservation in land plant anthers (Musial and Koscinska-Pajak, 2017; Sager and Lee 2018; Seale, 2020).

In this study, I aim to uncover the importance of callose polysaccheride in the initiation and progression of male meiosis. I will demonstrate that OsGSL5 is responsible for the accumulation of callose in anther locular cells in premeiotic and meiotic stages. The knockout of GSL5 resulted in the complete lack of callose deposition in premeiotic and meiotic anthers, as a result severely disrupted several key meiotic events such as meiotic mode of chromosome behavior, homologous synapsis and timely entry and progression of meiosis cell cycle, particularly meiosis I division. In the later part, I will focus on the cell-cell signaling aspects of callose, particularly during the mitosis-meiosis transition stages and propose that callose influence on male meiosis initiation and progression is likely due to perturbations in the symplastic and apoplastic pathways. Over all, my study will demonstrate that OsGSL5 is responsible for hyper callose accumulation in extracellular spaces of anther locules at premeiosis and early meiosis, in addition to the role in late meiosis and pollen development as previously reported (Shi et al. 2015), and has an indispensable role in proper initiation of male meiosis in rice, likely by controlling symplast and apoplast pathways.

Results

OsGSL5 impacts on pollen viability and seed fertility: To probe the importance of callose for male meiosis progression, we first selected the loss-of-function mutant of *OsGSL5* from the *Tos17* mutant panel (Miyao et al. 2003). The *Tos17* line selected in this study harboured a mutated *Osgsl5* allele hemizygous for *Tos17* retrotransposon insertion into the OsGSL5 protein-coding region ($Osgsl5^{tos17}$). Unfortunately, though 600 individuals in total obtained by self-pollination of the plants hemizygous for the *Tos17* insertion were genotyped by PCR, +/+ and $+/Osgsl5^{tos17}$ plants were only obtained in the 1:1 ratio. No segregation of homozygous $Osgsl5^{tos17}/Osgsl5^{tos17}$ plants suggests that the $Osgsl5^{tos17}$allele causes male gametophytic lethality, and is transmitted to the next generation only from female gametes.

Thus, I exploited CRISPR-Cas9 strategy to directly induce biallelic mutations in the *OsGSL5* genomic locus. Out of 32 CRISPR-edited plantlets screened, I obtained two independent knock-out lines, *Osgsl5-2* and *Osgsl5-3*, in which 1bp (A) was inserted on the 25th exon and 2bp (TA) were deleted on the 14th exon, respectively (Fig. 5A), resulting in frameshift mutations in both mutant lines. Both *Osgsl5* mutant lines were largely comparable to wild type (WT) plants in vegetative growth and panicles and spikelets morphologies under the same condition (Fig. 5B, C), except for two weeks-later heading compared to WT plants. However, both lines set no seeds; while WT plants had 63% fertility (Fig. 5C Table 2). Pollen viability was 0.5% and 1.2% in *Osgsl5-2* and *Osgsl5-3*, respectively, whereas it was 90.4% in WT (Figs. 5D, 6). These results are largely consistent to those previously reported (Shi et al. 2015). Expression levels of *OsGSL5* transcripts were significantly low at different anther development stages in CRISPR knock-out lines compared to the WT (Fig. 5E). Considering downregulation of *OsGSL5* transcription and reduced fertilities of pollen and seeds similarly in two independent lines, I concluded that CRISPR-Cas9-mediated frameshift mutations within *OsGSL5* coding sequence caused all above phenotypes. The anther length is broadly utilized as a standard to assess meiotic events in many angiosperm species including rice, as it has a rough collinearity with respective meiotic stages (Itoh et al. 2005) (Fig. 1). To confirm that *Osgsl5* mutant anthers retain this collinearity, I examined the expression profiles of two tapetum-specific genes, *TIP2* (Fu et al. 2014) and *EAT1* (Niu et al. 2013). The expression peaks of both genes appeared at a similar level in both WT and *Osgsl5-2* anthers (Fig. 7A). Noteworthily, the anther lengths where bimodal peaks of *EAT1* gene (Ono et al. 2018) arose were comparable (Fig. 7A), and further, no difference in the layered structure of meiotic anthers was observed between WT and both *Osgsl5* plants (Fig. 7B). These results indicate that the *Osgsl5* mutation unlikely affects the collinearity between anther lengths and meiotic stages, in addition to earlier anther morphogenesis. Thus anther

length was utilized as a standard for comparison of meiotic events between WT and *Osgsl5* mutants below.

OsGSL5 impact on callose accumulation in premeiotic and meiotic anthers: I monitored the detailed pattern of callose accumulation in rice meiotic anthers by aniline blue that specifically stains β-1,3-glucan chains. The callose amount in WT anther locules, which was at an undetectable level during mitotic SPC stage (Fig. 8A), started to fill the extracellular spaces between cell walls and cell membranes at both PMC-PMC junctions and PMC-TC interfaces (Fig. 8B). When PMCs entered into meiotic leptotene and zygotene, callose deposition was limited to PMC-PMC junctions (Fig. 8C, D). At subsequent pachytene to diakinesis stages, it can be seen enclosing PMCs with rounder shape (Fig. 8E-G). At dyad and tetrad stages, callose was detected on newly formed equatorial cell plates in addition to outer cell surfaces (Fig. 8H-I). After release of microspores to anther locules, callose can be seen fully enclosing microspores (Fig. 8J). In contrast, both *gsl5-2* and *gsl5-3* anthers displayed an extremely diminished callose signals through all premeiotic and meiotic stages observed (Fig. 8K-T).

To further assess the function of PMC-PMC junction as the callose producing center, a beginning stage of callose accumulation was observed with anti-β-1,3-glucan (callose)-directed antibody, to trace differences in callose amount more sensitively. In young 0.4-mm or less WT anthers, four microsporangia of a same anther sometimes show different callose patterns with each other (Fig. 9), suggesting it as the very beginning of premeiotic callose accumulation. In this stage, locules frequently retained callose limited to PMC-PMC junctions (Fig. 9), implicating that premeiotic callose accumulation initiates around PMC-PMC junctions, but not at PMC-TC interfaces.

To further clarify this trend, I performed the transmission electron microscopic (TEM) analysis. In TEM images of 0.35-0.5mm WT anthers around premeiotic interphase where callose accumulation initiated at the locular center (Fig. 9), I often detected a varying apoplastic space along the PMC-PMC interface (Fig. 10). Here, I separated a contacting region of two neighbouring PMCs adhering to TCs into 13 bins, and the cell-cell distance was measured at each bin in both WT and *Osgsl5-3* anthers. In WT anthers, the PMC-PMC interface region proximal to the center of anther locule showed a dramatic increase in space between two neighbouring PMCs, while the distance between two PMCs was gradually narrowed towards the TC side (Fig. 10A&B). This observation is very similar to the callose deposition pattern appeared at the junction where PMCs meet during premeiotic interphase stage as shown in Fig. 9, suggesting that the center of anther locule serving as site for callose biosynthesis and that callose signals propagate towards the PMC-TC interface starting from PMC-PMC junction at premeiotic interphase stage.

In contrast, the *Osgsl5-3* mutant anthers at the same stage never showcased such feature in any of the anthers observed (Fig. 10A). The cell-cell distance was widened uniformly at PMC-PMC and PMC-TC contacting regions, and the variation in cell-cell distances alongside with the central proximal-to-distal axis was completely disrupted (Fig. 10A&B). This results suggest that the cell-cell distances between PMCs is abruptly remodeled in absence of callose.

Localization of Callose and OsGSL5 protein in anther locules: To investigate spatio-temporal localization of OsGSL5 protein, I produced anti-OsGSL5 antiserum (Fig. 11) to perform co-immunostaining with the anti-callose antibody on anther sections. After initiation of callose accumulation at PMC-PMC junctions (Fig. 9), callose fulfilled extracellular spaces of both PMC-PMC and PMC-TC regions in anther locules (Fig. 12A), as observed in aniline blue staining (Fig. 8B). In contrast to callose staining, OsGSL5 localization was limited only at PMC-PMC junctions in the same anther section (Fig. 12A). In subsequent leptotene, the thick callose signal declined again at PMC-TC interfaces and became almost overlapped with OsGSL5 localization at PMC-PMC junctions (Fig. 12B-C). Through all stages observed, the strongest linear OsGSL5 signals were always observed at optically sectioned edges of PMCs (open arrowheads in Fig. 12), suggesting that OsGSL5 is a membrane spanning protein, well consistent to the fact that OsGSL5 and its orthologs are membrane-anchored proteins containing 15 transmembrane domains (Yamaguchi et al. 2004; Shi et al. 2015) (Fig. 11A). This trend became more obvious at subsequent pachytene-diakinesis stages, where PMCs gradually took a spherical shape (Fig. 12D-E). During these stages, OsGSL5 localization (Fig. 12D, E) was gradually corresponding to callose deposition on PMC surfaces (Figs. 8E-F, 12D-E). The OsGSL5 signal was at undetectable level in *Osgsl5* mutant anthers (Fig. 12A'-F'). These results strongly support that OsGSL5 takes part in callose biosynthesis during meiosis stages, and taken together with RT-qPCR results, reconfirm that the *Osgsl5* mutations are null alleles.

OsGSL5 impacts on male meiosis progression and chromosome behaviours: The chromosome behaviour was assessed at respective meiotic stages determined by both anther lengths and chromosomal morphologies on plastic-embedded sections. In WT, PMCs began meiotic chromosome condensation and displayed thin thread-like appearance by leptotene (Fig. 13A-C). Chromosomes were further condensed during zygotene (Fig. 13D), at which homologous chromosomes begin to be synapsed. At pachytene when synapsis is completed, PMCs displayed thick-threads of homologous pairs (Fig. 13E, E'). Bivalent chromosomes were further condensed through diplotene and diakinesis (Fig. 13F, G), and either of homologous pair was delivered to opposite poles during meta/anaphase I, and eventually to either cell of the dyad (Fig. 13H). In both *Osgsl5-2* and *Osgsl5-3* anthers, a conspicuous abnormality on

male meiotic chromosomes emerged during prophase I (Fig. 13I-O), in which two different types of PMCs were contained together within a same anther - one type carrying meiotic chromosomes with seemingly normal appearance, named WT-like PMC (wl-PMC) (Fig. 13L, M, M'_wl), and another displaying aberrant behaviors of meiotic chromosomes, such as tight aggregations and impaired homologous pairings, named aberrant PMC (ab-PMC) (Fig. 13L-O, M'_ab). The chromosome spreading method further clarified the abnormality in *Osgsl5* ab-PMCs (Fig. 14). During zygotene to diplotene, two types of PMCs were observed with respect to chromosome appearance in *gsl5* mutant anthers- the normal Wl-PMCs with fully synapsed chromosomes similar to the WT PMCs' chromosomes (Fig. 14A-J), and the ab-PMCs with chromosome aggregates (Fig. 14M-T). At diakinesis-metaphase I, unlike the WT PMCs where the 12 bivalents clearly observed and organized on equatorial plate, in *gsl5* mutant anthers, several univalent and multivalents like chromosomes were formed in addition to bivalents on the metaphase plate (Fig. 14U-X). This is consistent with the chromosome abnormalities observed by DAPI staining (Fig. 13).

In above observations, I noticed the *Osgsl5* mutation somewhat affected time-course progression of male meiosis, in addition to segregation of two PMC types. Thus, to make the *Osgsl5* impact on meiosis progression clearer, the frequency of each meiosis stage observed in PMCs was plotted along anther lengths. In 0.4- to 0.8-mm *Osgsl5* anthers, ab-PMCs appeared irregularly in range of 8.2-46.2% of all PMCs observed (Fig. 15A, Table 3). Another point of interest was a precocious initiation of several meiotic stages in not all, but a part of wl-PMCs, compared to WT PMCs. Interestingly, despite a subset of wl-PMCs displaying chromosomal features particularly of zygotene to dyad were observed earlier than WT PMC stages (asterisks in Fig. 15A), male meiosis was completed similarly in 0.9mm anthers of both WT and *Osgsl5* plants (Fig. 15A, Table 3).

In 0.4-0.5mm *gsl5* anthers, >85% of ab-PMCs retained chromosomal aggregates, and concomitantly appeared with diplotene/diakinesis-like wl-PMCs (Figs. 15B, 14M-V, Table S3). In 0.6-0.7mm *gsl5* anthers, about >27% of ab-PMCs had more condensed univalents and/or multivalents in addition to normal bivalents, concomitant with wl-PMCs retaining diplotene/diakinesis- or meta/telophase I-like chromosomes (Figs. 15B, 14O-V, Table 3). In 0.7-0.8mm anthers, >80% ab-PMCs again displayed less-condensed aggregated chromosomes concomitantly with diplotene/diakinesis-like wl-PMCs (Figs. 15B, 14O-V, Table 3). The reason was ambiguous, but it may suggest that aberrant aggregations of chromosomes at early prophase I resulted in uni/multivalent formation at later stages, and that ab-PMCs retaining uni/multivalents were abortive and undetected during late prophase I.

***Osgsl5* mutation caused precocious initiation of male meiosis:** An earlier occurrence of meiotic prophase-I stages frequent in *Osgsl5* anthers (Fig. 15) raises a possibility that it is attributable to defects

in premeiotic events. To test this hypothesis, I performed immunostaining of three meiotic initiation markers viz., PAIR2, PAIR3 and REC8 (Fig. 16). Rice PAIR2 promotes homologous chromosome synapsis, and its accumulation within the nucleus is reported to initiated during premeiotic interphase, just followed by the initiation of premeiotic DNA replication (Nonomura et al. 2006). Thus, PAIR2 can be used as a maker to infer the timing of replication initiation in anthers at premeiotic interphase. PAIR3 and REC8 are a chromosome axis protein and a meiotic cohesion subunit protein respectively, and both proteins are required for proper PAIR2 loading onto meiotic chromosome axes (Wang et al. 2011; Shao et al. 2011), thus these can serve as ideal markers for meiosis initiation time.

PAIR2, PAIR3 and REC8 nucleoplasmic signals were classified into three classes by their intensity; absent (class I), faint (class II) and strong (class III) (Figs. 16A, C). The PAIR2 class II is supposed to be a stage following premeiotic replication initiation. In WT 0.30-0.45mm anthers observed, 80% of PMCs showed no PAIR2 signal (class I), suggesting the cells being at mitotic SPC stage or before replication, and only 20% showed class II signals. In contrast, in anthers with the same lengths, around 60-70% of *Osgsl5* PMCs showed either class II or III signals (Fig. 16A), suggesting the precocious initiation of meiotic S-phase in *Osgsl5* PMCs. Similarly, PAIR3 and REC8 signals were quantified according to their appearance time in *Osgsl5* compared to WT (Fig. 16B, C). In 0.40-0.45mm anthers observed, 65% of WT PMCs showed no PAIR3 signal (class I), and 35% showed either class II or class III signals. In contrast, in same anther stage, 52-100% of *Osgsl5* PMCs showed either class II or III signals (Fig. 16C). In the same anther stages as above, REC8 class II or class III signals were observed in 39% WT PMCs. However, *Osgsl5* PMCs displaying class II or class III signals ranged from 58%-98% (Fig. 16C). These results clearly indicate that OsGSL5 has an impact on timely initiation of premeiotic events such DNA replication and formation of meiosis-specific chromosomal axes.

***Osgsl5* mutation disrupts homologous synapsis:** Next, I asked whether key meiotic events such as homologous chromosome synapsis was affected in *Osgsl5* PMCs or not. PAIR2 was normally loaded on meiotic chromosomes in both WT PMCs (n=168) and *Osgsl5-2* PMCs observed (n=134) (Fig. 17A), which further ensured that premeiotic accumulation of PAIR2 in PMC nuclei occurs normally even in *Osgsl5* mutants (Fig. 7). In contrast, loading of ZEP1, which is a transverse filament component of synaptonemal complex and governs meiotic crossover numbers in rice (Wang et al. 2010), was severely diminished in all *Osgsl5-2* PMCs at zygotene and pachytene (n=85), while it was constantly observed in all WT PMCs in same stages (n=92) (Fig. 17B).Though a chromosomal aggregate characteristic of ab-PMCs was hard to be distinguished at these stages, the result suggests that failed ZEP1 loading took place in both wl- and ab-PMCs in *Osgsl5* anthers.

Telomere bouquet is a chromosomal arrangement important for meiotic homologous pairing and synapsis in many eukaryotes including rice (Zhang et al. 2017). In anthers around leptotene and zygotene, only 37% PMCs displayed the bouquet in *Osgsl5-2* mutant (n=52), while 78% did in WT (n=41) (Fig. 17C). In 0.60-0.70mm anthers, no bouquet was observed both in WT and *Osgsl5-2* mutant (Fig. 18), suggesting the *Osgsl5* mutation restricted bouquet formation, but not dissolution.

Altered transcript levels of key meiotic and callose metabolizing genes in *Osgsl5* anthers: The transcriptional levels of 6 genes having key roles in meiosis initiation and two genes involved in callose metabolism were quantified in meiotic anthers by RT-qPCR. Of 6 genes, *Lepoto1* and *AM1* were significantly upregulated at premeiosis (0.3-0.4mm anthers). *MEL1*, *SPL* and *PAIR2* expression is also upregulated in young anthers compared to WT (Fig. 19).

Noteworthily, two callose metabolizing genes, *Osg1* gene encoding a tapetum-specific β-1,3-glucanase (Wan et al. 2011) and *UGP1* gene encoding an UDP-glucose phosphorylase involved in biosynthesis of cell wall components including callose (Chen et al. 2007), were both downregulated in *Osgsl5-2* anthers through all meiotic stages (Fig. 20), indicating a positive feedback regulation of OsGSL5 on callose metabolism related genes including *Osg1* and *UGP1*.

Callose contributes to the stability of plasmodesmata: In anthers at the SPC stage before the premeiotic interphase, all anther locular cells including PMC walls enriches cellulose (β-1, 4 glucan polymer) polysaccharide, and are interconnected with each other via PDs. As the PMCs enter into the meiosis cycle, their cellulose walls are gradually degraded and PMC walls majorly comprised of callose during premeiotic interphase and meiosis (Fig. 21). In parallel, the PD channels connecting PMCs and TCs also gradually disappear towards male meiosis, and PMCs are symplastically isolated for the later meiosis stages (Sager and Lee, 2018). Given the ability of callose to mediate cell-cell signalling via modulating the PD dynamics in plants, I asked whether depletion of hyper callose accumulation in premeiotic anther locules will impact the regular PD distribution in the *Osgsl5* mutant anthers or not.

To answer this question, I evaluated PD frequencies at three cellular interfaces in anther locules, viz., PMC-PMC, PMC-TC and TC-TC respectively, in anther locules by transmission electron microscopy (TEM). The anthers at three stages, stage1 (≤0.4mm), stage2 (0.45mm) and stage3 (≥0.5mm) roughly corresponding to the mitosis, premeiosis and meiosis stages, respectively (Fig. 1), were observed for PD frequency in both WT and *Osgsl5* anthers. In WT anthers, the PD density was high during stage1 (anther ≤0.4mm), but then gradually reduced as PMCs transit from mitosis to meiosis (stage2&3) (Fig. 22). This observation is in line with the previous observations in anthers (Heslop-Harrison, 1964; Mamun et al.

2005; Mursalimov et al. 2010; Mursalimov et al. 2013; Radice et al., 2008). However, in *Osgsl5* mutant anthers, the PD density was reduced relative to WT at all three cellular interfaces observed in anthers during the mitosis-meiosis transition (Fig. 22 right). At stage1 (anther ≤0.4mm), the PD numbers at PMC-PMC and PMC-TC interface are significantly low in *Osgsl5-3* anthers compared to the WT anthers (Fig. 22). Similarly, at stage2&3 (anthers >0.4mm), the PMC-PMC and PMC-TC interface PDs also reduced but not significantly (Fig. 22 right). At TC-TC interface, the PDs remained comparable between WT and *Osgsl5-3* anthers at stage1, however, at later stages, (anthers >0.4mm), PDs reduced strikingly, but not completely abolished. These observations strongly imply that in the absence of callose, the PDs are likely unstable and disintegrate prematurely, and thus callose likely contribute to the stability of cytoplasmic connections between anther locular cells during mitosis-meiosis transition.

Callose is required to maintain appropriate apoplast spacing among anther locular cells: Above observation and the dramatic increase of space between PMCs-PMCs at regions corresponding to callose deposition sites (Fig. 9 &10), prompted me to ask how the callose depletion influences the apoplastic space at all three intercellular spaces. To answer this question, I quantified the apolastic space at all cellular interfaces in both WT and mutant anthers. In WT anthers, as PMCs progress from premeiosis stage to meiotic prophase I stages, the angular PMCs become spherical, and move apart with each other, resulting in an increase of apoplastic spaces in WT anther locular cells. As expected, the apoplastic space between PMC-PMC and PMC-TC increased in WT meiotic anthers (stage2 anther >0.5mm) compared to mitotic anthers (stage1, anther <0.45mm), while the TC-TC space remained unchanged (Fig. 23A, B). I asked the question if callose depletion can impact the spacing between anther locular cells in the *Osgsl5* mutant anthers or not. Surprisingly, the increment of apoplastic spaces was enhanced more in *Ogsl5* anthers compared to the wild type at PMC-PMC interface specifically at stage1 (Fig. 23A,B&C), while the cell-cell distance at stage2 didn't enhance further as would be expected for PMCs progressing into meiosis (Fig. 23A,B&C). The apoplastic space in other cellular interfaces remain mostly comparable to that of WT anthers (Fig. 23A,B&C). These observations raise a possibility that callose deposition may contribute to keep moderate apoplastic distances between PMCs only during mitosis-meiosis transition, probably for facilitating the apoplastic signalling among PMCs and TCs. As an alternative possibility, the PDs and cell-cell distance may interconnected. PDs when remain intact, may keep the PMCs closure but when these channels are disintegrated they release the PMCs to move freely within locules, resulting increased apoplastic space between PMCs as seen in *gsl5* anther locules lacking callose and reduced PDs (Fig. 10, 22&23).

Discussion

OsGSL5-dependent callose accumulation in rice anthers during meiosis

This study gained important insights into OsGSL5, an anther-specific callose synthase, responsible for hyper-callose accumulation at extracellular spaces of anther locules during premeiotic and meiotic stages (Fig. 8). Double immunostaining of OsGSL5 and callose revealed that subcellular OsGSL5 localizations are restricted on PMC plasma membrane facing to PMC-PMC junction, where multiple PMCs meet with each other along the central axis of anther locules, and served callose polysaccharides to extracellular spaces of PMC-PMC junctions through premeiosis and early prophase I (Fig. 12A-D). Another important point is that during premeiotic interphase stage, specifically, the callose deposition was observed at PMC-TC interfaces in addition to PMC-PMC junctions, whereas OsGSL5 localization was very much limited to PMC-PMC junction (Fig. 12A). Given that callose accumulation begins at PMC-PMC junctions, but not at PMC-TC interphases (Fig. 9), callose synthesized at PMC-PMC junction is likely supplied for fulfilling PMC-TC interfaces during premeiotic interphase, further affirming PMC-PMC junctions as a callose-producing center, while the factors responsible for the diffusion of callose polysaccharide remains a open issue.

Fluctuation in callose levels, as above mentioned, generally involves two counteracting enzymatic activities: β-1,3-glucan synthases and hydrolases (Frankel et al. 1969; Stieglitz and Stern, 1973). A rice β-1,3-glucanase, Osg1, functions in timely callose degradation on pollen grains and impact on pollen fertility (Yamaguchi et al. 2002; Wan et al. 2011), and *Osg1* gene expression was reduced in *Osgsl5* mutant (Fig. 20), likely suggesting a positive feedback regulation of *Osg1* transcription by elevated callose levels to maintain callose homeostasis in anthers. Rice *UGP1* is a UDP-glucose pyrophosphorylase that catalyzes production of UDP-glucose, a substrate of glucan synthases, including OsGSL5. In *UGP1* RNAi plants, callose accumulation in anther was significantly diminished during both meiotic and post-meiotic stages (Chen et al. 2007) which is consistent with our results (Fig. 8). Thus, it is possible that UDP-glucose catalyzed by *UGP1* is used for *OsGSL5*-dependent callose synthesis, leading to callose accumulation during meiosis and post-meiosis, and *Osg1* probably acts in callose fluctuation antagonistically to the UGP1-OsGSL5 pathway.

Impact of callose accumulation on male meiosis initiation

A key insight gained with this study is the impact of OsGSL5 on male meiosis initiation and progression (Figs. 13, 14, 15, 16). In addition to defects in meiosis time-course, *Osgsl5* mutant included ab-PMCs that exhibited several other defects in chromosome behaviour and condensation, homologous synapses

and reduced bouquet structures, along with wl-PMCs that exhibited a normal appearance of meiotic chromosomes (Figs. 13, 14, 15). Even if a part of *Osgsl5* PMCs passed through meiosis, callose deposition is defective also on all surviving tetrad spores (Fig. 8T), resulting in male sterility as previously reported (Shi et al. 2015).

Shi et al. (2015) concluded that OsGSL5 is responsible for callose accumulation at post meiosis stages, but not during early meiosis. However, this conclusion was led only by a snapshot of whole-mount staining of anthers with aniline blue, but not of sectioning, perhaps resulting in an oversight of OsGSL5 impact during premeiotic interphase and prophase I stages. Similarly, a frequent appearance of survival spores, probably derived from wl-PMCs, may explain the reason why the impact of callose function during male meiosis was underestimated in previous studies using mutant plants lacking callose synthesis.

Microscopic observations of *Osgsl5* mutant PMCs implicated that wl-PMCs with meiotic chromosomes lacked ZEP1 loading (Fig. 17B), but achieved seemingly normal bivalent formation and disjunction of homologous pairs in meiosis I (Fig. 14K, L). It is not surprised, because in rice *zep1* mutants, bivalents were formed at the normal level and a considerable number of tetrads were formed, while the viability of gametes significantly reduced probably due to aberrant chromosomal condensation in microspores (Wang et al. 2010). Rather, it is a wonder why meiotic chromosomes of *Osgsl5* wl-PMCs loose the capacity for ZEP1 loading. Furthermore, frequent appearance of ab-PMCs is difficult to be explained only by the loss of ZEP1, because of no appearance of such aggregates reported in *zep1* mutants (Wang et al. 2010). A similar loss of ZEP1 loading is observed in *mel2* mutant PMCs (Nonomura et al. 2011), in which *OsGSL5* expression is significantly reduced (Fig. 3). Furthermore, PMCs at various cell cycle stages segregated in a same *mel2* anther, due to asynchronous initiation of DNA replication (Nonomura et al. 2011). This observation may account for appearance of two different PMC types in *gsl5* anthers (Figs. 13, 14), taking place together with precocious male-meiosis entry (Fig. 16). Rice LEPTOTENE1 (LEPTO1), a type-B response regulator that participates in establishing key features of meiotic leptotene chromosomes. In *lepto1* mutant anthers, expression levels of both *OsGSL5* and *UGP1* genes were reduced significantly and callose depleted during meiosis (Zhao et al. 2018). Interestingly, the loading of important meiotic chromosome elements, such as OsREC8, OsAM1 and ZEP1, was also defected in *lepto1* (Zhao et al. 2018). The past observations and findings of this study together strongly implicate that callose filling the extracellular spaces of anther locules is an important step for proper PMC differentiation and/or male meiosis initiation, while the underlying mechanisms have been remained elusive.

Callose influence on male meiosis initiation likely by affecting symplast and apoplast pathways

The above observation findings have clarified two important things about the relationship between

callose metabolism and PD dynamics in plant system. First, the disintegration of intercellular connections during mitosis-meiosis transition (Heslop-Harrison, 1964; Mamun et al. 2005; Mursalimov et al. 2010; Mursalimov et al. 2013), likely independent of callose deposition as observed in *gsl5-3* anthers (Fig. 22), thus denying the previously held hypothesis that callose deposition being direct cause of PD destruction in anthers (Sager and Lee, 2018). Though it is currently unknown how the PDs dissolution is achieved during mitosis to meiosis transition. One likely possibility of that the PD disintegration may be developmentally regulated due to progressive maturation of anthers. Second, callose may contribute to transient stability of PDs before they are gradually shutdown by current unknown factors. Transient stability or maintenance of PDs perhaps is required to allow symplast communication related to meiosis initiation among anther locular cells as suggested by previous reports (Plackett et al. 2014; Zhai et al. 2015; Liu et al. 2017; Huang et al. 2019; Lei and Liu 2020). Future experiments involving cell-cell diffusion experiments may be necessary to fully support this claim. In addition to controlling symplastic pathway, callose accumulation is thought to function as a molecular filter for signalling from TCs to PMCs via apoplastic pathway (Clement & Audran, 1995; Roschzttardtz et al. 2013). Biochemical evidence further suggest that callose deposition can alter permeability and plasticity of cell walls in coexistence with cell-wall components like cellulose (Abou-Saleh et al. 2018). With PDs gradually disappearing in anther locules during mitosis-meiosis transition, PMCs may switch to the apoplast path to communicate with neighboring locular cells (Roschzttardtz et al. 2013). In this context, maintaining an appropriate distance between cells in anther locules is critical for the apoplast system to remain functional. The increase in apoplastic spaces was observed to a greater extent in *Osgsl5* mutant anthers than in WT at PMC-PMC (Fig. 10&23), suggesting that callose deposition may help to maintain the appropriate spacing between PMCs, probably for facilitating apoplastic signaling between them after their symplastic isolation. The above findings imply that hyper callose accumulation has a potential to bring dramatic microenvironmental changes to its surrounding PMCs by affecting controlling symplastic or apoplastic pathways or both.

Callose may aid in SPC/PMC cell shaping during mitosis-meisois transition

Another intriguing finding of this study is that PMCs attained globose shape in both presence and reduced callose in anther locules. In angiosperms, the soma- and germ-cell niche in stamens and carpels share a common lineage (Goldberg et al. 1993), However, only the primordial germ cells (archesporial cells), which are mostly trapezoid or rectangular-shaped having no curvy sides at their inception, become extremely enlarged in size/volume relative to surrounding somatic cell-niche, and attain globose shape as they mature and progress into meiotic prophase I stages (Kelliher & Walbot, 2011; Ouedraogo et al. 2023). Although, recently an organ level control on germ cell shape and size is proposed (Ouedraogo et

al. 2023), the underlying mechanics responsible for such dramatic transformation of germ cells morphology over the course of time is largely unknown.

In this study, the electron microscopic images, taken at around early premeiotic interphase stages, showcased a typical callose deposition starting from locule center (PMC-PMC junction) where cell-cell distance is enhanced at regions corresponding to callose deposits (Fig. 9&10). However, this feature is radially narrowed down towards TC side corresponding to the reduced callose signals their (Fig. 9&10). Given that callose deposition begins at the locule center, the square/rectangular/trapezoidal shaped germ cells may initially transform into angular shape with curvy edges at the center corresponding to callose deposit site (Fig. 10), and as the callose signals propagate along PMC-PMC side towards the PMC-TC side and fills completely (Fig. 8B&9A), the PMCs shape is also tweaked accordingly. Eventually, during meiotic prophase I stages, with an extremely high amount of callose deposited at the central locules (Fig. 8C-G&9B-E), the PMCs are fully transformed into a more spherical/globose shaped PMCs and become isolated inside the locules (Fig. 8F-G). Therefore, I propose that callose at the central locule may directly aid in shaping the morphology of SPCs/PMCs during mitosis-meiosis transition and subsequent prophase I stages. If it was the case, the angular shaped PMCs at the center of locule is expected to never be rounded in *Osgsl5* anthers (Fig. 10). Actually, during leptotene stage, the *Osgsl5* PMCs kept rectangular or trapezoidal shape even at the central corner, while WT PMCs become curvy at the center corresponding to callose deposit (Compare Fig. 8C&M), suggesting that my proposal is likely until this stage. However, in subsequent stage, PMCs eventually become spherical shaped in both WT and *Osgsl5* mutant anthers (Fig. 8N-P). Hence I would like to point out that, in addition to callose, some unknown genetic mechanisms may also collectively contribute to sculpture the cell shape and volume of SPCs/PMCs, either directly or indirectly. This may explain the globose PMCs formed in absence of callose in *Osgsl5* anthers, and that callose is one of multiple factors/forces contributing to the morphogenesis of reproductive cells. In budding and fission yeasts, cell-size mediated cell cycle arrest is operative (Hartwell, 1974; Nurse, 1975). In smaller cells, the activity of Wee1 is kept active and cdc2, a driver of mitotic entry, is arrested. When the cells elongate and attain certain size threshold, Wee1 inhibition on cdc2 is lifted and mitosis is initiated (Lundgren et al. 1991; Russel & Nurse, 1987). Reduction in cell size also delays the DNA replication initiation in *E. coli* (Hill et al. 2012). The fact that enormous enlargement of SPCs size prior to meiosis entry suggests a similar cell size threshold mechanism also existing for meiosis entry in plants. In this view, callose-mediated PMCs shaping observed at the locule center (PMC-PMC junction) may serve as a localized cue for timely initiation/entry of DNA replication/meiosis cycle. A schematic model showing PMC shaping by callose during mitosis-meiosis transition is shown in Fig. 24.

Conclusion

During the transition from mitosis to meiosis in flowering plants, an extensive remodeling of germ cell walls takes place, whereby the cellulosic-rich PMC walls are drastically rearranged and replaced by callose (Matsuo et al. 2013, also see Fig. 21). Such hyper callose accumulation in anther locules, referred to as "histological hallmark" of PMCs entering meiosis, marks the initiation of meiosis division in sexual plants, while it was enigmatic as to why such drastic turnover of PMCs wall composition from cellulose to callose is required during mitosis to meiosis transition time. In this study, I have demonstrated that callose deposition in premeiotic and meiotic anthers is dependent on GSL5. In the absence of callose, the initiation and progression of meiosis is strongly affected with *Osgsl5* mutant anthers mostly lacking callose showcased precocious initiation and progression of meiosis, accompanied by several meiosis defects in chromosome condensation, behavior and homolog synapses (Figs. 8, 12, 13-16). The formation of aggregates of chromosomes during mid-late prophase I stages may reflect uneven/abnormal maturation of crossover intermediates. In the absence of ZEP1, the number crosssovers (CO) elevate several species studied thus far including budding yeast, rice, *Arabidopsis* and *C. elegans* (Bachelier et al. 2011; Libuda et al. 2013; Wang et al. 2015; Voelkel_meiman et al. 2016). Depletion of ZEP1 on meiotic chromosomes may suggests a similar CO elevation happening in absence of synaptonemal complex in *Osgsl5* lines. Estimation of CO numbers in these lines may yield deeper insights into the relationship between callose and recombination events in plants. Another fascinating thing that remains unknown at this moment is the leaky behavior of callose specifically during premeiotic interphase stage, whereby the callose polysaccharide seen diffusing away from the site of production (PMC-PMC junction) to PMC-TC junction (Fig. 12A). The β-1,3-glucans are proposed to have gel-like properties in a pH dependent manner, whereby an alkaline condition can induce callose gel-formation, whereas an acidic environment makes glucans a rigid polymer (Harada et al. 1968; Saito et al. 1977; Eggert et al. 2014). Local regulation of apoplastic pH by vesicles, together with the cellulose concentration, could also influence callose physical properties and drive its movement within apoplast space (An et al. 2006; Voigt et al. 2014; Abou-Saleh et al. 2018).

I next attempted to investigate how callose actually impacts male meiosis initiation and progression in rice. Recent studies have suggested the role of callose accumulation in male meiosis via cross-talking among anther locular cells via symplast and/or apoplast pathway (Plackett et al. 2014; Zhai et al. 2015; Liu et al. 2017; Huang et al. 2019; Lei and Liu 2020). In young anthers before meiosis onset, the

cytoplasm of all anther cells, including SPCs, PMC initials and TCs, are all connected with each other by PD channels (Heslop-Harrison, 1964; Mamun et al. 2005; Mursalimov et al. 2010; Mursalimov et al. 2013; Radice et al., 2008). However, during transition to meiosis, interconnections of PMC-TC and PMC-PMC are thought to be solved/blocked, probably by hyper callose accumulation (Sager & Lee, 2018). With the disintegration of symplastic pathways, the PMCs continue to communicate with neibouring cells via apoplastic signaling pathway (Roschzttardtz et al. 2013). To investigate whether hyperaccumulation of callose in premeiotic anther locular cells can influence the symplast and/or apoplastic communication I examined the anthers at mitosis to meiosis transition stage in WT and *gsl5-3* anthers by transmission electron microscopy. My findings show that the dissolution of PDs takes in *gsl5-3* mutant anthers at PMC-PMC, PMC-TC and TC-TC junctions. This observation is contrary to the previous conception that callose deposition being a direct cause of PD disintegration in anther and therefore propose that callose maintains PD stability rather than a constrain to PD numbers during mitosis-meiosis transition. Further, my results also indicate that callose deposition is required to maintain proper apoplastic spacing among anther locular germ cells, perhaps this phenotype is intertwined with the PD numbers. Presence of PDs stabilized by callose can potentially hold the PMCs intact, thereby minimizing the space between the cells, and allows a smoother switch of cell-cell signaling system from symplast to apoplast pathway during mitosis-meiosis transition. Whereas, the callose absence may cause destabilization and disintegration of PDs prematurely and disrupt the normal flow of symplast to apoplast switch accounting for meiosis defects absence in the subsequent stages (Fig. 14&15). In addition, the callose may directly be involved in PMC cell shaping starting from the center of locule and reflects a drastic cell-wall remodeling happening between PMCs, including PD reduction and apoplast space increase. Taken together, the findings of this study show that GSL5-dependent callose deposition in premeiotic and meiotic anthers is required for proper male meiosis initiation and progression, thereby shedding light on the mitosis–meiosis transition control machinery, while leaving behind some fundamental clues for future research works to follow.

Material and Methods

Plant materials and growth conditions: For target mutagenesis of *OsGSL5* gene (*Os06g0182300*), potential CRISPR guide-RNA sequences were designed using CRISPR-P v2.0 software (Liu et al. 2017). Double stranded DNAs were produced from oligo DNA pairs of gRNAF1/gRNAR1 and gRNAF2/gRNAR2 for *Osgsl5-2* and *Osgsl5-3* (Table S2), respectively, by annealing. After cloning into

pU6 vector, the *pU6* promoter-fused double-stranded DNA was transferred to pZD shuttle vector (Mikami et al. 2015), and introduced into seed-derived calli of *japonica* rice cultivar Nipponbare by the method previously reported (Hiei et al. 1994). All plants were grown in growth chambers at 30˚C day and 25˚C night temperature and 70% relative humidity with a daylength of 12 hours.

Pollen and seed fertility tests: For pollen fertility, the panicles were fixed in carnoy's fluid and anthers were extracted from fixed panicles and were squashed on the microglass slide. The squashed anthers were stained in I_2-KI solution for 10 min. The viable pollen grains stained dark and non-viable lightly stained pollen grains were counted under the light microscope BX50 (Olympus). For calculating the seed fertility, the ratio of fertile spikelet numbers was counted in each of five panicles and averaged to get the average seed setting percentage (%) plant.

Cytological observations: For observations of chromosome behaviours and callose deposition on anther sections, anthers were fixed in 4% paraformaldehyde (PFA)/1xPBS in vaccum for 80 min. Panicles were checked for every 20 min interval for 80 min. Vaccume fixed samples were then shaked for 2 hours in Ice and wash with 1x PBS buffer for 15(x6) min to completely replaced PFA with 1x PBS buffer. Samples were kept at 4^0C until for further experiments or used immediately. After removal of lemma and palea of florets, anthers were dehydrated in ethanol graded series (30%, 50%, 70%, 90% and 100%) for 30-60 min each, followed by infiltration in embedder with hardener1 of Technovit 7100 (Kulzer Technique), overnight on rotor at 4˚C. The solution was replaced with fresh Technovit with hardener1 every 6 hours and incubated overnight with on rotor at 4˚C. Then, anthers were transferred to a cryo-dish with Technovit polymerised by addition of harderner2 and placed at 50-60˚C for hardening. Plastic embedded sections with 4-6µm thickness were taken using the microtome R2255 (Leica), and air dried at room temperature. The section was stained for 25-30 min with 0.01% aniline blue (Sigma Aldrich) in 0.1M K_3PO_4 (pH 12) for callose, or with a drop of 1.5µg/mL 4',6-diamidino-2-phenylindole (DAPI)/Vector shield (Vectorlabs) for chromosome observation. The images were captured under the confocal laser scanning microscope system FV300 (Olympus), and processed with ImageJ (https://imagej.nih.gov/ij/docs/intro.html).

For chromosomal spreads, whole panicles were fixed in Carnoy's fluid and stored at 4˚C until use. Fixed anthers were incubated with 0.1% $FeCl_2$ overnight. Next day anthers were squashed in acetocarmine solution (1% (w/v) carmine (Merk)/45% acetic acid) with forceps on a clean glass slide. After quick removal of anther-wall remnants, a suspension of released PMCs was covered with a cover slip, and gently heat-treated followed by gentle thumb compression. The images of chromosomal spreads were captured under the light microscope BX50 with DP2-SAL CCD camera system (Olympus). The

number of PMCs each classified by certain phenotypes in chromosome behaviours was counted and used for quantification together with those observed in plastic-embedded sections.

RT-qPCR: To quantify the transcript levels of rice genes, anthers and tissues were collected from fresh samples, and immediately frozen in liquid nitrogen in a 2mL tube with 2mm beads. The samples were then homogenized on automated shaker BMS-A20TP (Bio Medical Science) at 1100rpm for 2min. RNAs were extracted by TRIZOL RNA extraction kit method according to manufacturer's instruction (Invitrogen) and supplied to Super Script III First-Strand synthesis system (Invitrogen) for cDNA library construction using the oligo dt primers. RT-qPCR was performed using Real Time System TP800 (TAKARA bio systems), according to manufacturer's instruction. All primer sequences used for RT-qPCR were shown in Table S2. *Rice Actin1* (*RAc1*) gene was used as an internal control to normalize the expression levels at all meiosis stages quantified.

Antibody production: To produce an antibody specific for OsGSL5 of 1910 amino acids (aa), the cDNA sequence encoding 1009-1260 aa position was amplified using the above cDNA library as a template (Fig. 11), and cloned into pDEST17 vectors (Invitrogen). The His-tagged protein expressed in *E. coli* strain BL21-AI (Invitrogen) was purified using Ni-NTA agarose resin (FUJIFILM), and immunised to rabbits and guinea pig.

To observe telomere behaviours in PMCs, the antibody was raised against rice PROTECTION OF TELOMERE1 (OsPOT1), which is encoded by a single gene locus *Os04g0467800* (*LOC_Os04g39280.1*), while Arabidopsis genome has two paralogous loci, *POT1a* and *POT1b* (Shakirov et al. 2005). Procedures to raise antisera are same as above.

Immunofluorescent staining of PMCs and tissue sections: Young rice panicles were fixed with 4%PFA/1xPMEG (25mM PIPES, 5mM EGTA, 2.5mM MgSO4, 4% glycerol, and 0.2% DMSO, pH 6.8), followed by washing 6 times with 1xPMEG, and stored at 4˚C until use (Nonomura et al. 2006). For immunofluorescence of PMCs, fixed anthers were treated with the enzyme cocktail of 2% cellulase Onozuka-RS (Yakult)/0.3% pectolyase Y-23/0.5% macerozyme-R10 (FUJIFILM Wako)/0.375% Cytohelicase (Sigma-Aldrich) in 1xPME (same with 1xPMEG except for excluding glycerol) for permeabilization on MAS-coating glass slide MAS-02 (Matsunami Glass), squashed by forceps and used for immunostaining, as described in Nonomura et al. (2006).

Immunostaining of anther sections was done as described by Tsuda and Chuck (2019) with minor modifications. Briefly, anthers were dehydrated in ethanol graded series and Histo-Clear (Cosmo bio co. Ltd), embedded into Paraplast paraffin wax (McCormick Scientific). Paraffin blocks containing anther

samples were trimmed and stored at 4˚C until use. The blocks were sectioned into 8-10µm thickness by the microtome. Dewaxed and rehydrated samples were incubated with primary antibodies. The rabbit anti-OsGSL5, the rabbit anti-OsPOT1 (this study), the rabbit anti-PAIR2 (Nonomura et al. 2006), guinea pig anti-PAIR3 (Wang et al. 2011), anti mice-REC8 (Shao et al. 2011) and rat anti-ZEP1 antibodies (Nonomura et al. 2011) were diluted to 1/100, 1/3000, 1/3000, 1/200, 1/200 and 1/1000, respectively, with 3%BSA/1xPMEG and used as primary antibodies. For callose immunostaining, monoclonal antibody specific to β -1,3-glucan (callose) (Biosupplies Australia) was diluted to 1/1000 and used as a primary antibody.

In both squash and sectioning methods, secondary antibodies Alexa fluor 488 (Abcam) and Cy3-conjugated IgG (Merck) of 1/200 dilution was used for detection. Immunofluorescent images were captured by Fluoview FV300 CSLM system (Olympus) and processed with ImageJ.

Transmission Electron Microscopy: Rice florets at various meiosis stages were collected and fixed in 4% PFA in 1x PBS buffer. Again fixation in 1% PFA and 2.5% GA in 0.05M PBS buffer. Sample was washed in PBS buffer and florets post-fixed in 2% (w/v) osmium tetraoxide (OsO4) in 0.05M PB for 1 hour on Ice. Dehydration is done in ethonal series (30 min each), propylene oxide (30 min) and lastly with resin Quetol 812 (120 min and 12 hours) at room temperature on rotator. Next day, Embed to the pure resin at 37C for 120 min. Again embedding done with the pure resin (Quetol 812) at 37C for 60 min. Flat-embed with Quetol 812 on the silicon-coated slide glasses or put in a flat embedding mold, and incubated at 70C for 48hours. Resin block is trimmed and ultrathin sections of 100-150nm were made. Sections first stained with 4% w/v uranyl acetate for 10 min and Lead Stain Solution (Sigma-Aldrich) for 5 min. Sections were observed under Transmission electron microscopy (JEM1010).

Quantification of PD frequencies and PMC-PMC distances on TEM images: PD numbers at different anther stage sections was counted and normalized against the cell wall length at a given cell-cell interface to obtain the percent PDs observed/µm cell wall length. The statistical significance of PD frequency at each cellular interface between WT and *Osgsl5-3* anthers was calculated by Student's t-test. The average cell-cell distance at PMC-PMC, PMC-TC and TC-TC interface was taken in different anther stage sections and further averaged to obtain the overall mean cell-cell distance of that floret at each interface. A contacting region of two neighbouring PMCs both adhering to TCs is divided into 13 bins, and the PMC-PMC distance was measured at each bin in both WT and *Osgsl5-3* anthers. Mean TC-TC distance of each floret was almost comparable between WT and *Osgsl5-3* anthers, and thus used to normalize the PMC-PMC and PMC-TC distance of each section derived from the same floret. The

statistical significance of cell-cell distance at each cellular interface between WT and *Osgsl5-3* anthers was calculated by Mann Whitney's U test.

Gene accession numbers: Gene accession numbers used in this study are displayed in Table 4.

Acknowledgement

With immense pleasure and profound sense of gratitude, indeed, I take this opportunity to express my heartfelt and sincere thanks to my esteemed supervisor, **Dr. Kenichi Nonomura**, Plant Cytogenetics Laboratory, National Institute of Genetics, for his meticulous guidance, indelible inspiration, persistent encouragement, ingenious suggestions, mellifluous nature and indefatigable attitude. I will ever cherish the fatherly affection that he bestowed upon me throughout my tenure as a student under him which helped me to cope with many difficult situations.

I owe my sincere thanks to co-superviser **Dr. Yutaka Sato** and the members of my advisory committee **Dr. Shin-ya Miyagishima, Dr. Kuniaki Saito, Dr. Noriyoshi Sakai** and also past committee members **Dr. Yoshihisa Oda** (Nagoya University) and **Dr. Yumiko Saga** (Emiretus, National Institute of Genetics) for their critical suggestions, impeccable and benevolent guidance.

I thank **Dr. Norio Komeda** (NIG, SOKENDAI) for helping the production of anti-OsPOT1 antiserum. I am thankful to **Dr. Keiko Takanami** and **Dr. Amane Oishi** (Koide lab) for their kind cooperation in teaching me the transmission electron microscopy, **Dr. Brent Gowen** (University of Alberta, canada) for his helpful suggestions in microscopic imaging and **Dr. Yoselin Benitez-Alfonso** (Leeds University, United Kingdom) for her helpful suggestions with TEM data analyses.

The mel2 mutant used in this study was provided by NIG with support from National BioResource Project (NBRP) Rice, AMED, Japan. This work was partly supported by JSPS KAKENHI Grant No. 21H04729 and 18H02181 (to K.I.N), and Bilateral Programs Grant No. JPJSBP120213510 (to K.I.N).

I extend my indebtedness to the members of the Nonomura lab for their discerning comments, valuable suggestions, co-operations and helpful attitude towards me during the course of investigation.

I owe my sincere thanks to all the staff members of National Institute of Genetics for their keen interest taken in the work providing the necessary and timely research facilities, inspiration and suggestion throughout the work.

With profound regards in a more personal sense, I owe deepest debts to my father **V Somashekar** and my mother **Lakshmidevamma**, my sister **Aadhya Pavan** and my brother in-law **Pavan Kumar Baidyshetty**. It was their constant encouragement, moral and emotional support rendered throughout my education for which I will remain indebted to them throughout my life.

I offer my sincere thanks from the core of my heart to **MEXT (**Ministry of Education, Culture, Sports, Science and Technology) for providing me financial support throughout my doctoral study.

Last but not the least, I record my sincere thanks to all respectable people who helped me and could not find separated mention. I still solicit their benediction to proceed at every step of a perfect destined life.

Figures

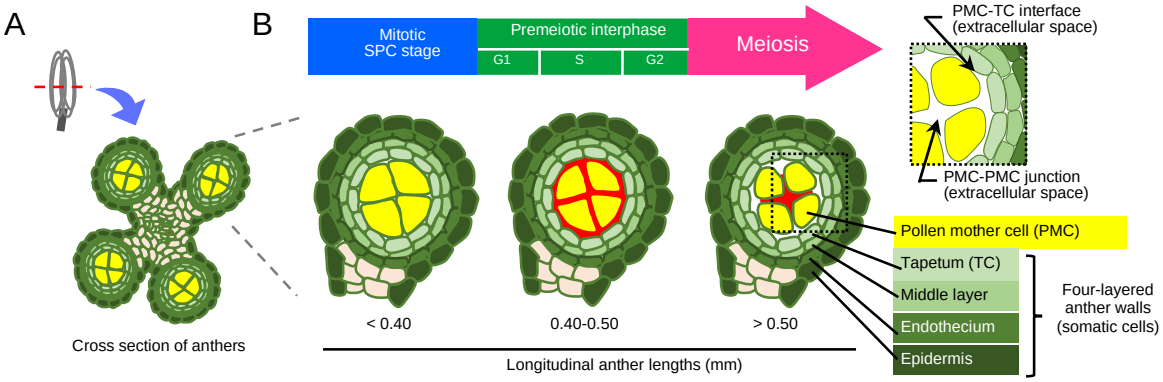

Figure 1. Schematic illustration of anther development and callose accumulation during male meiosis progression. A: Illustration of a cross section of premeiotic anther with four locules. B: Enlarged view of anther locules with constituent cell types, respective anther lengths and their cell cycle status. The red regions in each locule correspond to areas for callose deposition at extracellular spaces observed in this study.

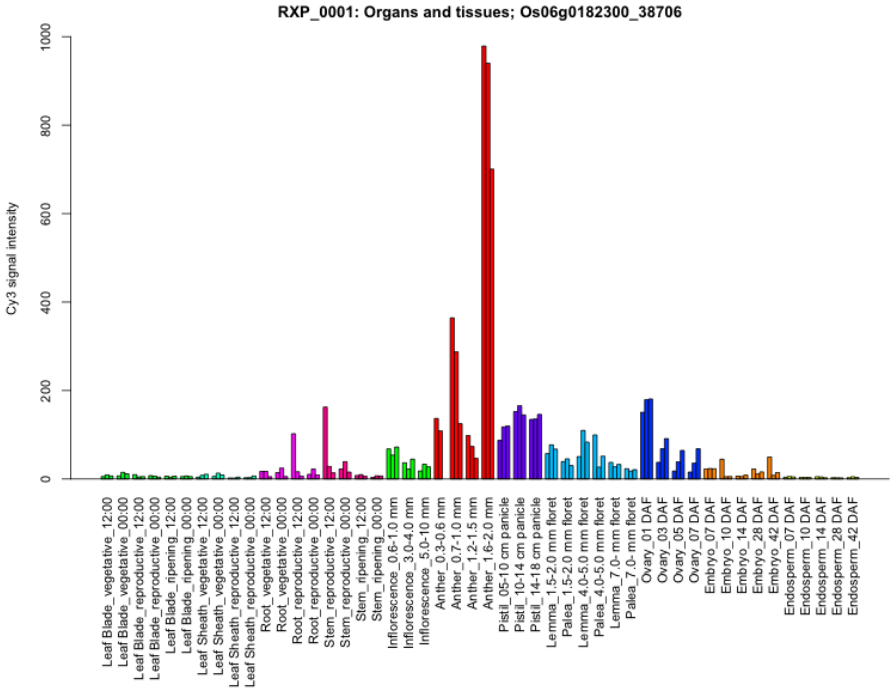

Figure 2. Expression profile of *OsGSL5* gene at various tissue developmental stages in wild type (WT) rice plants. The data was downloaded from the online database RiceXPro

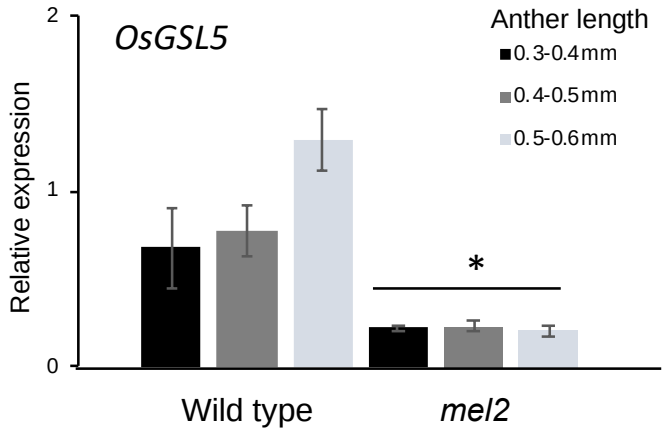

Figure 3. Transcript levels of *OsGSL5* gene quantified by RT-qPCR in wild type (WT) and *mel2* anthers. Errors bars indicate a standard deviation of the mean of three biological replicates. Anthers from >10 florets were collected and used in each replicate in RT-qPCR. Asterisks indicate significant differences *(*P*<0.05 by Student's *t*-test) between WT and *Osgsl5-2*.

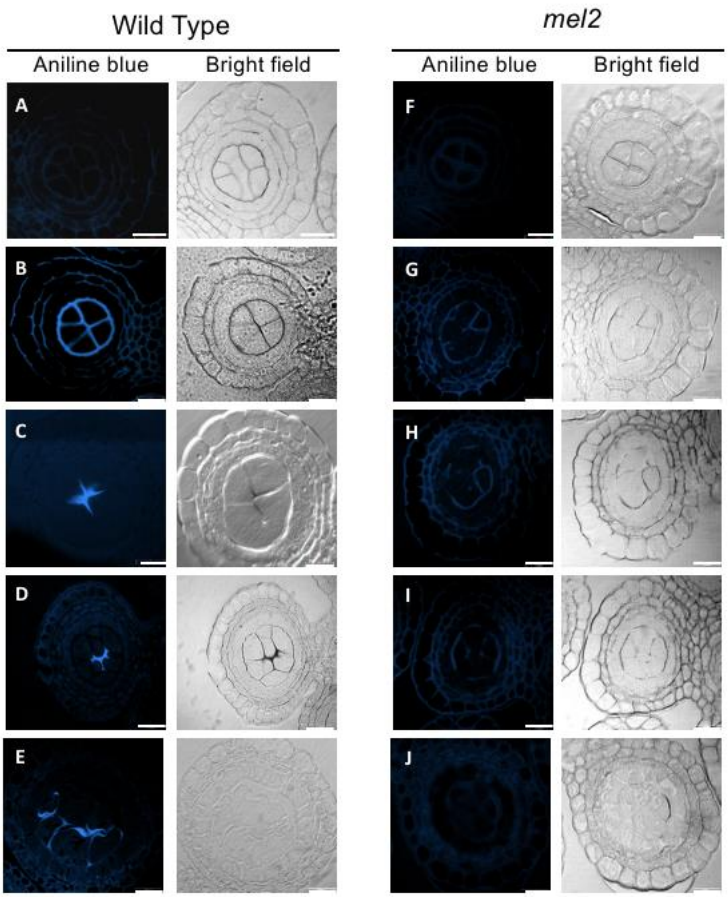

Figure 4. Callose accumulation in wild type (WT) and *mel*2 anthers. Aniline blue staining revealed reduction of callose in *mel2* mutant anthers compared to WT. A and F: Mitotic SPC stage, B and G: Premeiotic interphase, C and H: Leptotene-Zygotene, D and I: Pachytene, E and J: Diplotene-Diakinesis. Bar=20um.

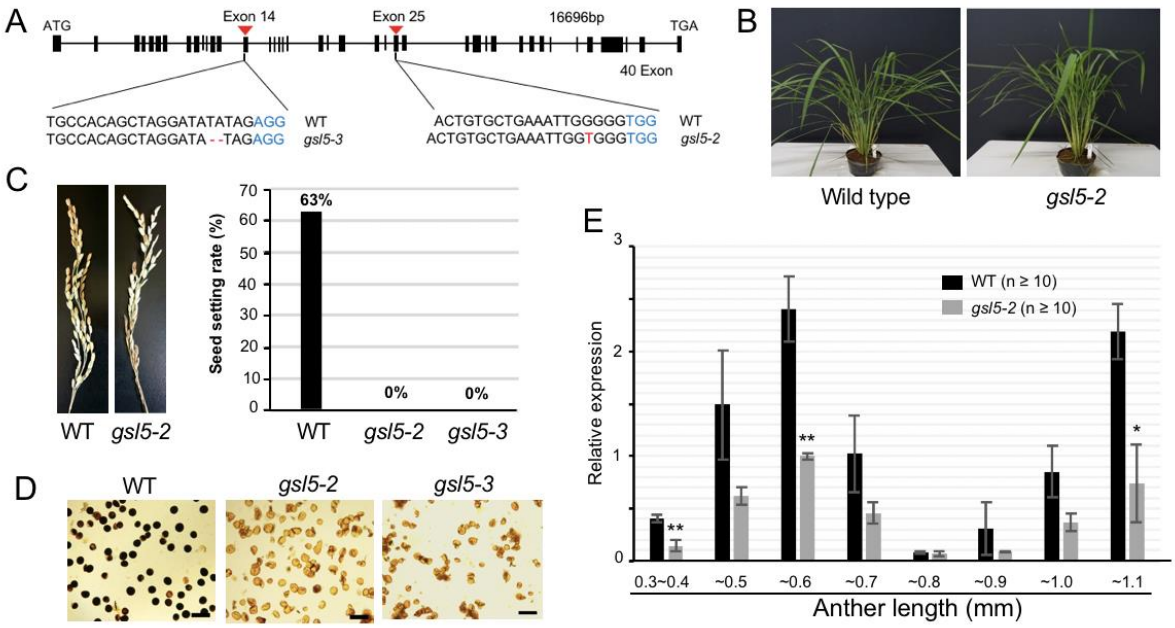

Figure 5. The *osgsl5* mutant phenotype and *OsGSL5* gene expression. A: Nucleotides deletion and insertion sites in *Osgsl5-2* and *Osgsl5-3* knock-out mutants. B: The vegetative plant growth was comparable between wild type (WT) and *Osgsl5-2*. C: Images of panicles at seed filling stage of WT and *Osgsl5-2* (left), and the graph showing seed setting rate of WT, *Osgsl5-2* and *Osgsl5-3* (right). D: Pollen viability test by KI_2 staining of WT (left), *Osgsl5-2* (middle) and *Osgsl5-3* (right). Darkly and faintly stained grains were categorized as viable and nonviable pollen, respectively. Bar=40μm. E: The relative expression levels of *OsGSL5* transcripts in WT and *Osgsl5-2* anthers by RT-qPCR. Errors bars each indicate the standard deviation of the mean of 3 biological replicates. The n value in parentheses is the number of florets used in each replicate. Asterisks indicate significant differences (*P<0.05, **P<0.01 by Student's t-test) between WT and *Osgsl5-2*.

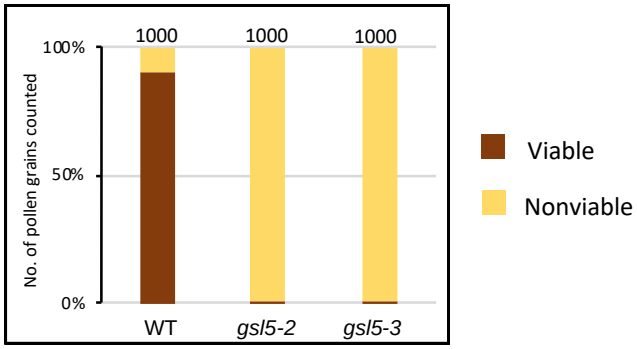

Figure 6. Pollen viability quantification in wild type (WT) and *Osgsl5* mutants. The number at the top of each bar indicates the absolute number of pollen

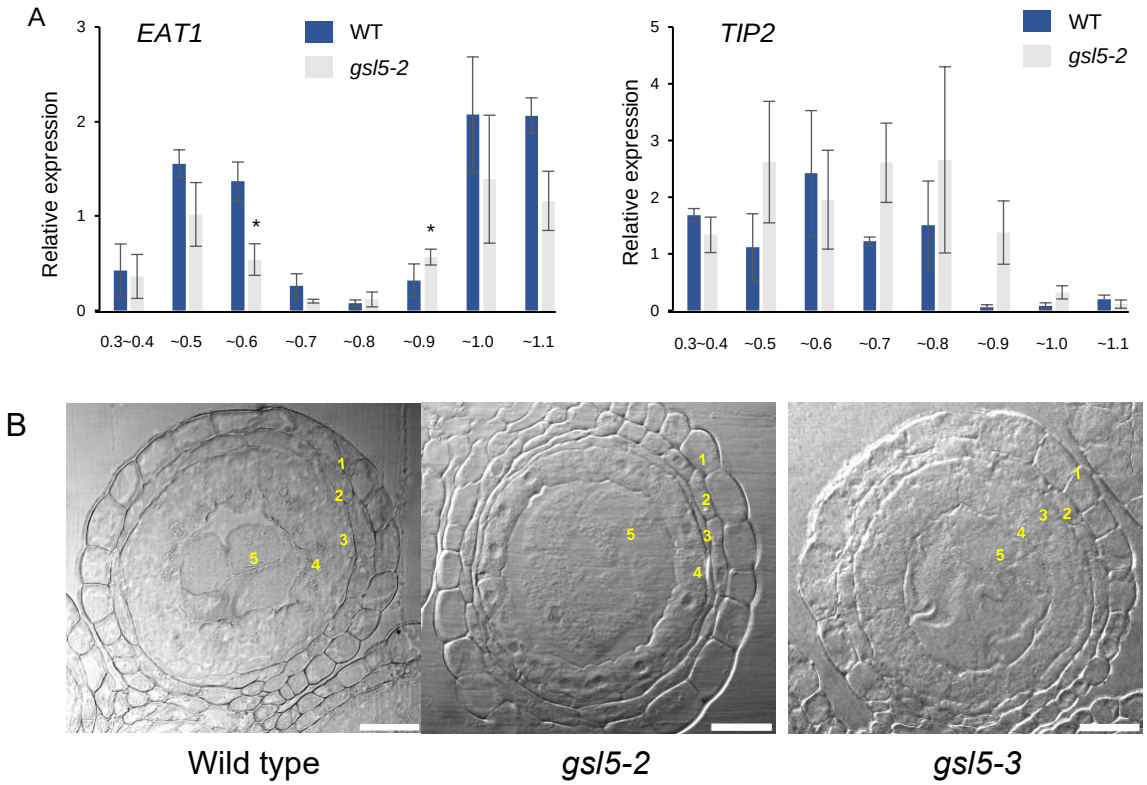

Anther Layers

1. Epidermis, 2. Endothecium, 3. Middle layer, 4. Tapetum, 5. Pollen mother cell

Figure 7. Anther development is unaffected in *Osgsl5* mutants. A: Transcript levels of tapetum specific genes *EAT1* and *TIP2* in wild type (WT) and *Osgsl5-2*. Errors bars indicate a standard deviation of the mean of three biological replicates. Anthers from >10 florets were collected and used in each replicate. Asterisks indicate significant differences *(*P*<0.05 by Student's *t*-test) between WT and *Osgsl5-2*. B: Comparison of anther morphology at diplotene-diakinesis stage (~0.6mm anther) between WT, *Osgsl5-2* and *Osgsl5-3*. Bar=20µm.

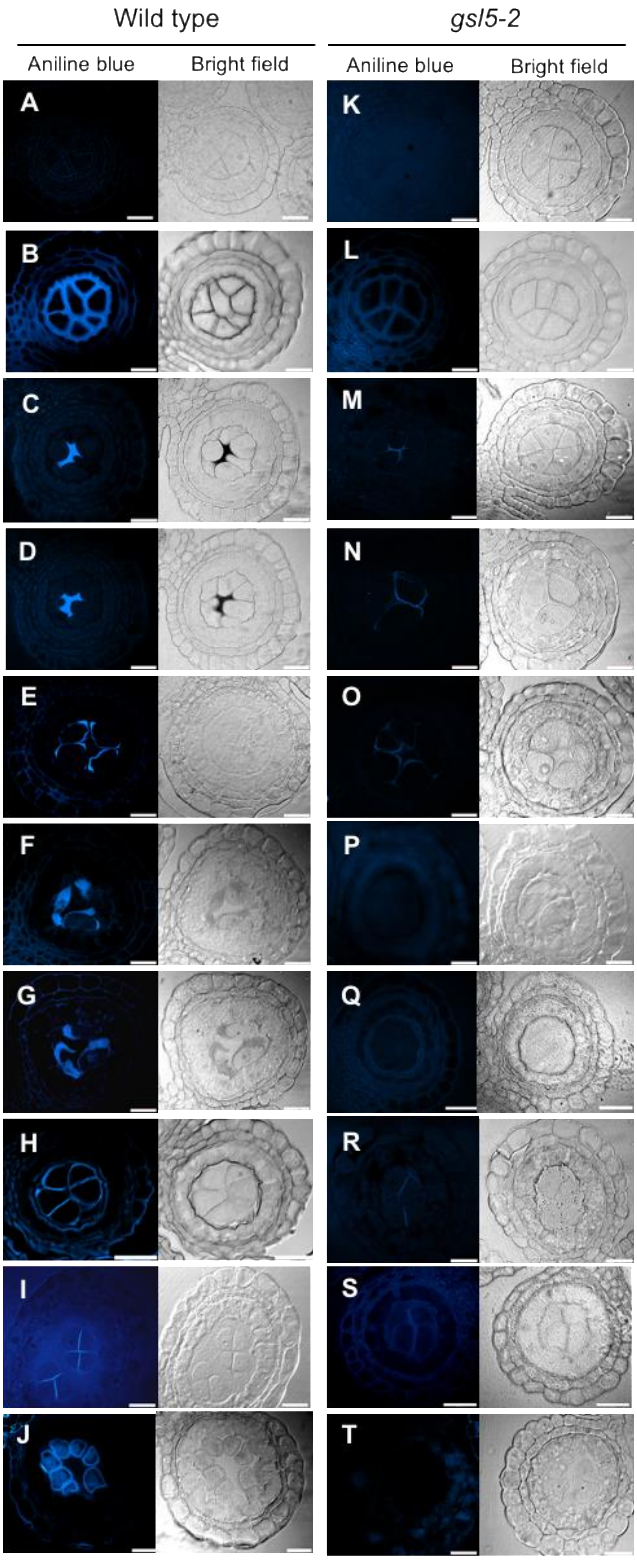

Figure 8. Callose accumulation during male meiosis in wild type (WT) and *Osgsl5-2* anthers. Callose accumulation pattern was monitored by aniline blue staining at different male meiosis substages. A and K: Mitotic SPC stage, B and L: Premeiotic interphase, C and M: Leptotene, D and N: Zygotene, E and O: Pachytene, F and P: Diplotene, G and Q: Diakinesis, H and R: Dyad, I and S: Tetrad, J and T: Microspore. An arrowhead in the inset in B indicates the cell wall unstained with aniline blue. Bar=20μm.

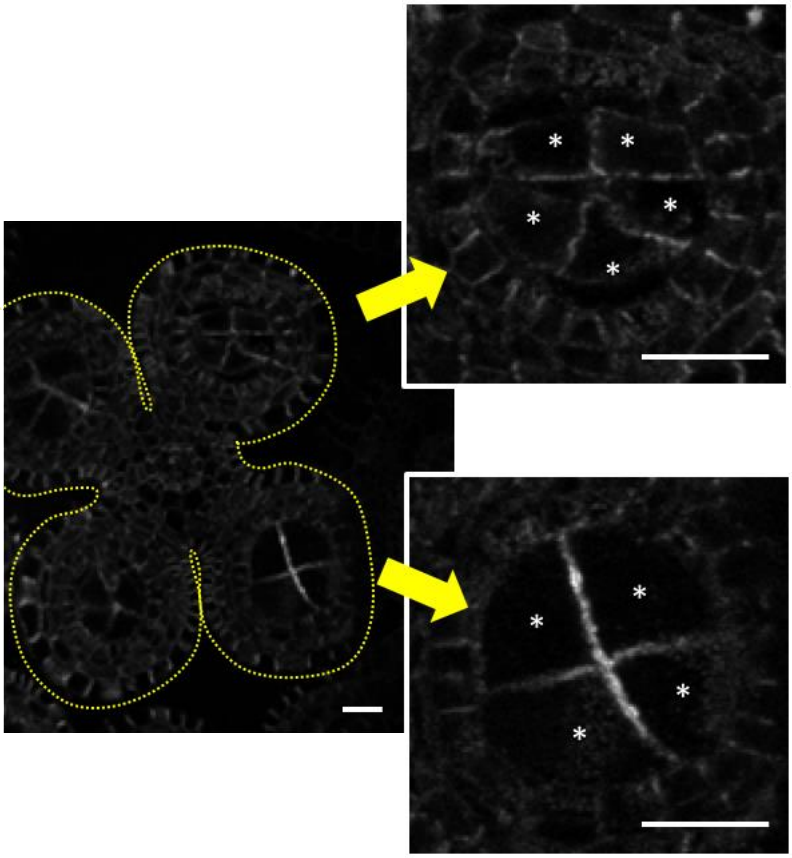

Figure 9. Callose deposition at its beginning stage during premeiotic interphase in wild type (WT) anthers. Callose deposition was immuno-stained with the anti-β-1,3-glucan antibody. Asterisks indicate the position of Pollen Mother Cells. This anther harbored both callose-absent (right top) and callose-present locules (right bottom), indicating it at the beginning of callose accumulation. Bar=20um

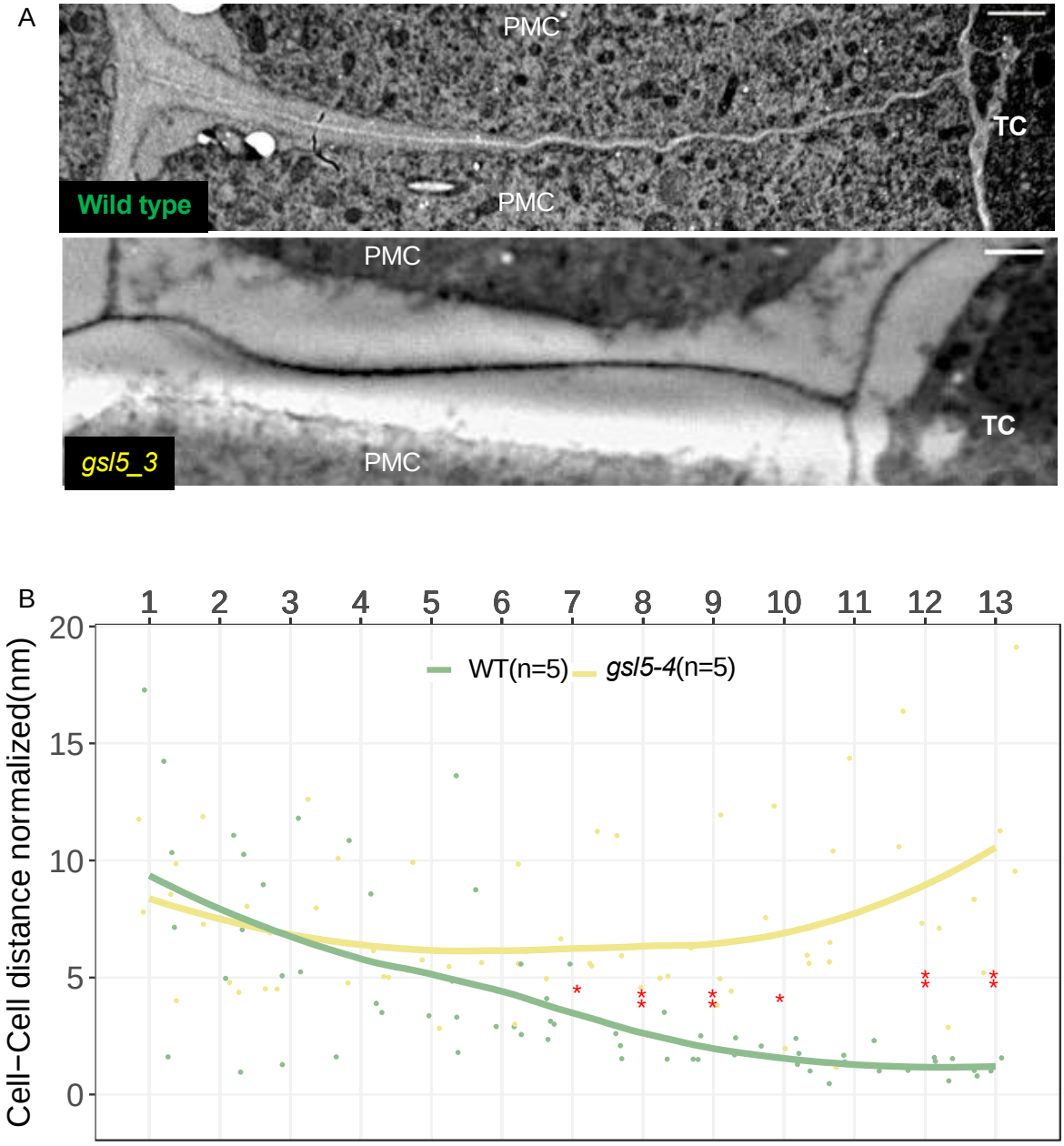

Figure 10: Varying apoplast space along PMC-PMC interface anticlinal to TC. A: Apoplast space observed along the PMC-PMC interface in anther central locule at premeiotic interphase stage accumulating callose. B: Quantification of the apoplast space observed along the PMC-PMC interface in WT and *gsl5-3*. Red asterisks indicate significant differences (*$p \leq 0.05$ by Mann Whitney's U Test) between WT and *Osgsl5-3*. Anther length measured 0.35-0.5mm. scale = 1um

A

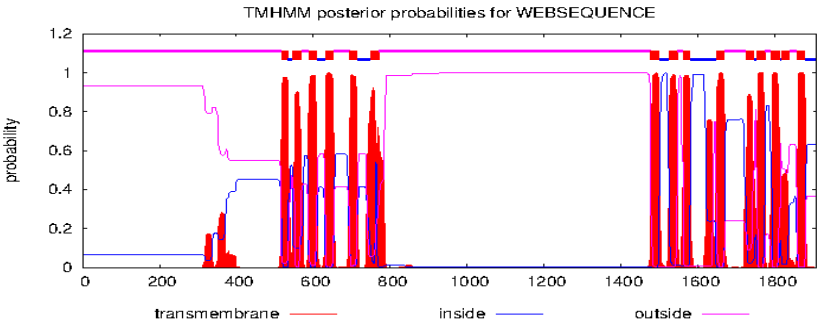

B

MTGPRGGGGEDPPRTSSGAAASASASSGVPNEPLTPTSMLMSGQQAGLNRRGSRSAAMATFSMEVFDNEV
VPSTLSSIAPILRVAAEIEPERPRVAYLCRFYAFEKAHRLDQNSVGRGVRQFKTALLQRLEKDNSPSLAKRVKKTD
AREIESFYQQYYENYVRALDKGEQADRAQLGKAYQTAGVLFEVLCAVNKNEKVEEVNPEIVRLHRDVQEKKDI
YTPFNILPLDAASASQSIMQMEEIKAAVAALRNTRGLTWPSTFEPERQKGGDLDLLDWLRAMFGFQRDSVRN
QREHLILLLANVHIRLEPKPEPLSKACSFATFYFADLTIWISMWIMKSPQGAQPQEIQQRNILFLGLYLLIWGEA
ANIRFMPECLCYIFHNMAYELNGLLAGNVSIVTGENIRPSYGGDEEAFLKKVVTPIYRVIKKESGKSKHGKTPHS
AWCNYDDLNEYFWTTDCFSLGWPMRDDGDFFKSVHDSRPVTTAGSSSQKGSTKSTGKMNFVETRTFWHIF
RSFDRMWTFYLLALQAMLIFAWSDYTLSQILQKDLLYSLSSIFVTAAFLQFLQSILDFVLNFPGHHKCKFLDAMR
NILKIIASAAWAVILPFFYISTASKVNLPIKDLDKWFQYVKGVPPLYILAVAVYLIPNILSAALFLLPCFRRWIENSD
WRIVRLLLWWSQKRIYVGRGMHESSVSLFKYTLFWILLLCSKFAFSYFVQIKPLIKPTKDIMNVHNIHYEWHEFF
PNASYNVGAVMSLWAPVLLVYLMDTQIWYAIFSTISGGVSGALGRLGEVSPSKRTEAAKFAQLWNEVICSFRE
EDLISDKEMDLLVVPYSSDPSLKLMQWPLFLLASKIPIALDMAAQFRPRDSDLWKRICADEYMKCAVLECYESF
KLVLNLLVIGENEKRIIGIIIKEIEANIAKNTFLANFRMSALPVLCKKFVELVSALKERDASKFDNVVLLLQDMLEVI
TRDMMVNEIRELAEFGHGNKDSVPRRQLFAGTGTKPAIVFPPPISAQWDEQIKRLYLLLTVKESAMDVPTNLE
ARRRIAFFTNSLFMDMPRAPRVRKMLSFSVMTPYYSEETVYSRNDLDLENEDGVSIIFYLQKIFPDEWNNFLERI
GCQRESEVWGNEENVLQLRHWASLRGQTLCRTVRGMMYYKRALKLQAFLDMASESEILEGYKAVADPAEEE
KKSQRSLSSQLEAIADMKFTYVATCQIYGNQKQSGDRRATDILNLMVNYPGLRVAYIDEVEERDGEKVQKVFY
SVLVKALDNHDQEIYRIKLPGPAKLGEGKPENQNHAIVFTRGEALQTIDMNQDNYLEEALKMRNLLEEFHENH
GVRQPTILGVREHIFTGSVSSLAWFMSNQETSFVTIGQRVLANPLKVRFHYGHPDVFDRIFHITRGGISKASCGI
NLSEDIFAGFNSTLRRGNVTHHEYIQVGKGRDVGLNQISLFEAKVACGNGEQTLSRDIYRLGHRFDFFRMLSCY
FTTVGFYISSMMVVIIVYVFLYGRLYLALSGLELAIMKQARMRGNTALQAAMGSQSIVQLGLLMALPMFMEIG
LERGFRSALGDFIIMQLQLCSVFFTFSLGTKSHYFGRTILHGGAKYKATGRGFVVRHVKFPENYRMYSRSHFVK
GLELMLLLVVYQMYGDVATDSTAYILLTSSMWFLVITWLFAPFLFNPSGFEWQKIVDDWDDWSKWISSRGGI
GVPANKAWESWWEEEQEHLQSTGFFGRLSEIILSLRFFIFQYGIMYHLNISAGNKSISVYGLSWLVIVAVVMVL
KVVSMGRKKFSADFQLMFRLLKLFLFIGSIGTLAILFTLLHLTVGDIFASFLAFAPTGWAILQISQASKPVVKAFGL
WGSVKALSRGYEYLMGILIFVPVAVLAWFPFVSEFQTRLLFNQAFSRGLQISRILAGGKKQS*

Vta1 (77-202aa)

FKS1 (352-463aa)

Glucan synthase (1032-1724aa)

Figure 11. OsGSL5 protein structure. A: The positions of transmembrane domains in OsGSL5 protein by TMHMM-2.0 software. B: A deduced amino acid sequence of OsGSL5 (1910 a.a.), in which peptide sequences of functional domains, Vta1, FKS1 and Glucan synthase domain, were colored. Fifteen transmembrane domains detected in A were marked with underlines, and the region used for the antigen in this study was with a doubled underline (252 a.a.).

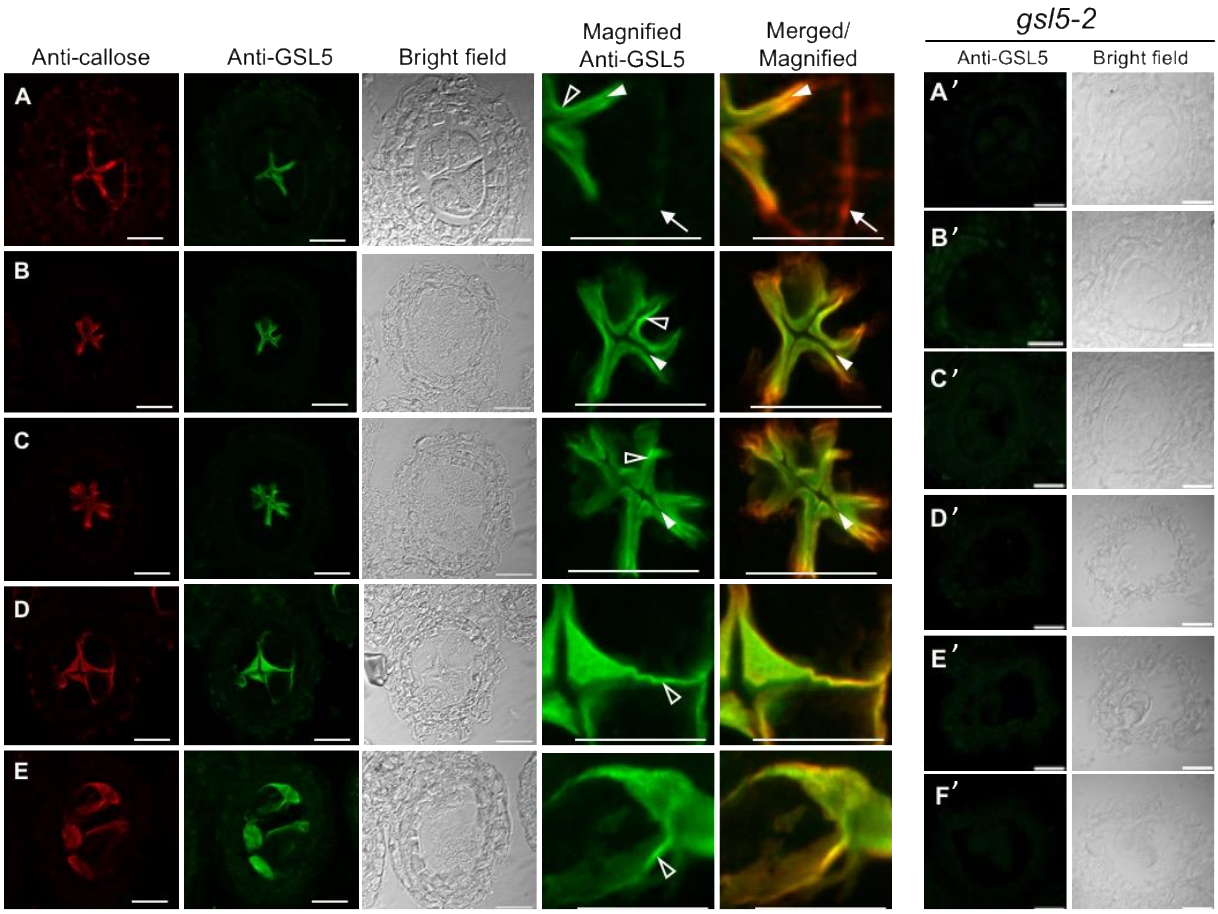

Figure 12. Co-immunostaining of callose and OsGSL5 protein in wild type (WT) anthers. A&A': Premeiotic interphase, B&B': Leptotene, C&C': Zygotene, D&D': Pachytene, E&E': Diplotene-Diakinesis. F': Dyad. Bar=20μm. In panel A, white arrows show the region retaining callose deposition (red), but lacking OsGSL5 localization (green), at Pollen Mother Cell (PMC) – Tapetal Cell (TC) interface. The closed and open arrowheads indicate unstained cell-wall regions and linearly aligned OsGSL5 signals on PMC plasma membranes, respectively. Sections of *Osgsl5-2* mutant anthers were immuno-stained with anit-OsGSL5 antibody (right).

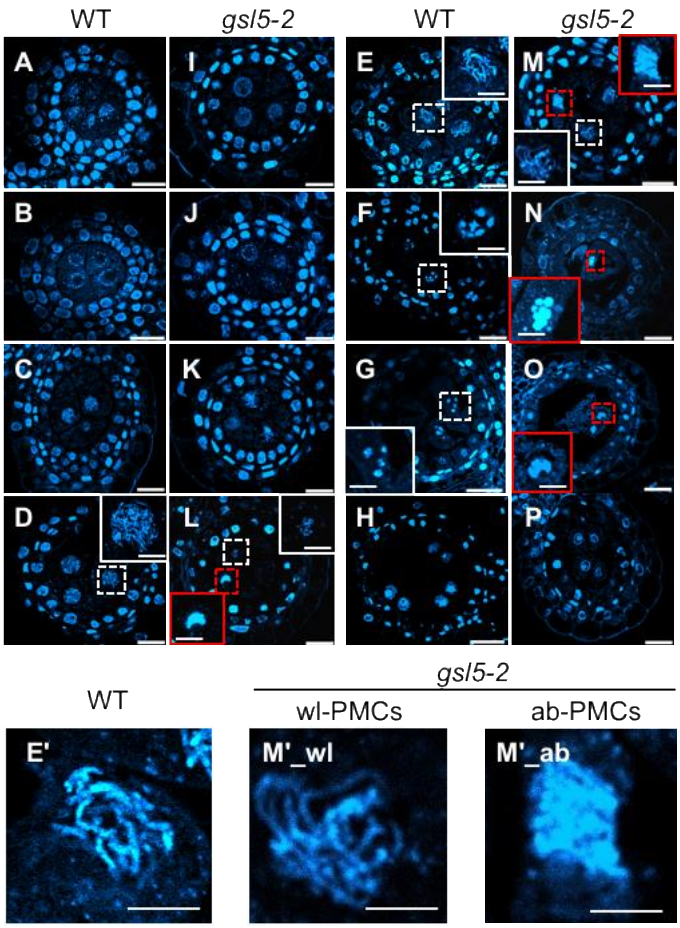

Figure 13. Dynamics of chromosomal behaviour in WT and *Osgsl5-2* anthers. Plastic-embedded anthers cross sections stained with DAPI for chromosomes observation. A and I: Mitosis, B and J: Interphase, C and K: Leptotene, D and L: Zygotene, E and M: Pachytene, F and N: Diplotene, G and O: Diakinesis, H and P: Dyad. Bar=20μm. Note that *Osgsl5-2* mutant anthers contained two types PMCs with respect to chromosome appearance (wl-PMC and ab-PMC, see the text). The insets in each panel are magnified views of nuclei enclosed with dashed squares, in which white and red squares indicate nuclei of wl-PMCs and ab-PMCs, respectively. The insets in panels E and M are further magnified and shown in E', M'1 and M'2, as examples of WT PMC, wl-PMC and ab-PMC.

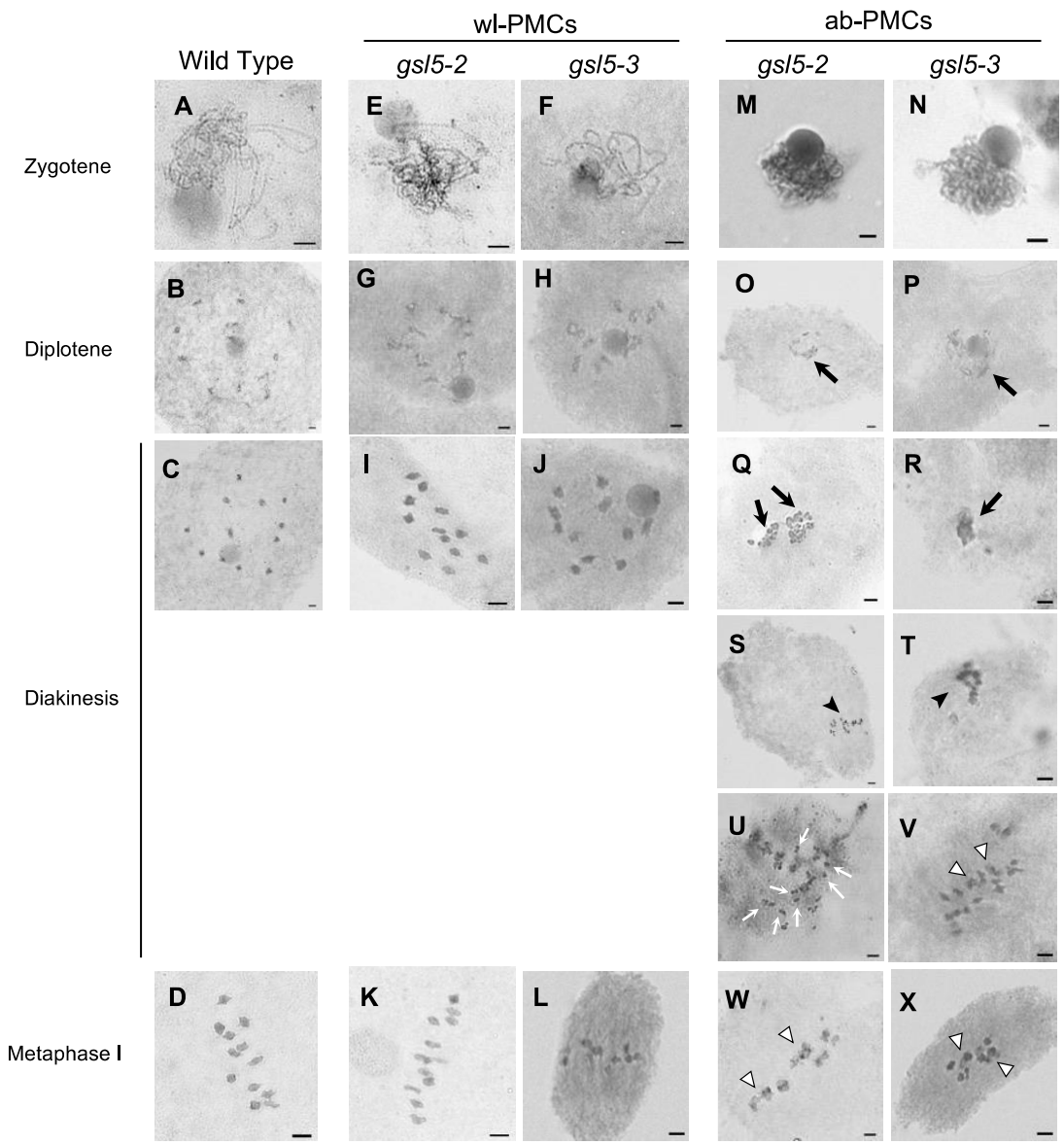

Figure 14. Aberrant chromosome behaviors detected in *osgsl5* mutant anthers by chromosome spreading technique. Both wildtype-like Pollen Mother Cells (wl-PMCs) and abnormal Pollen Mother Cells (ab-PMCs) were segregated in a same *osgsl5* anthers. Thick black arrows indicate aberrant chromosomal aggregates. Black arrowheads show chromosomal clusters that located near the cell peripheral region. White arrows and arrowheads indicate univalent and multivalent chromosomes, respectively. Bar=2.5μm.

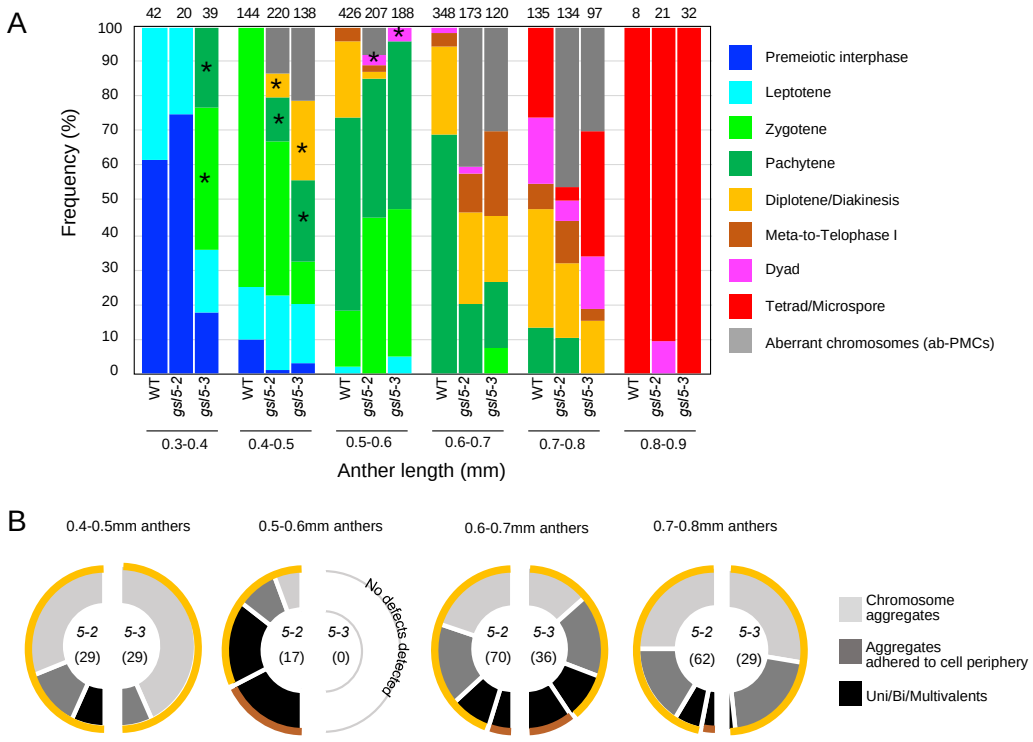

Figure 15. Male meiosis progression and ab-PMC appearance in wild type (WT) and *Osgsl5* anthers. A: Frequency of Pollen Mother Cells (PMC) stage observed with respect to anther lengths in WT and *Osgsl5* mutants, in which the frequency of aberrant (ab)-PMCs in *Osgsl5* anthers was shown as gray bars. The number at the top of each bar indicates the absolute number of cells counted. The wild type-like (wl)-PMC stages marked with asterisks indicate that those stages emerged much earlier than comparable stages observed in WT anthers. B: Each half-donut graph indicates frequency of three different classes for aberrant chromosomal morphologies and behaviors in *Osgsl5-2* or *Osgsl5-3* ab-PMCs observed along respective anther lengths. Colored outer rims on a half donut indicate meiotic stages of wl-PMCs that concomitantly emerge with respective classes of ab-PMCs. Definition of outer rim colors is consistent to that in A. The number in parentheses represents the absolute number of cells counted.

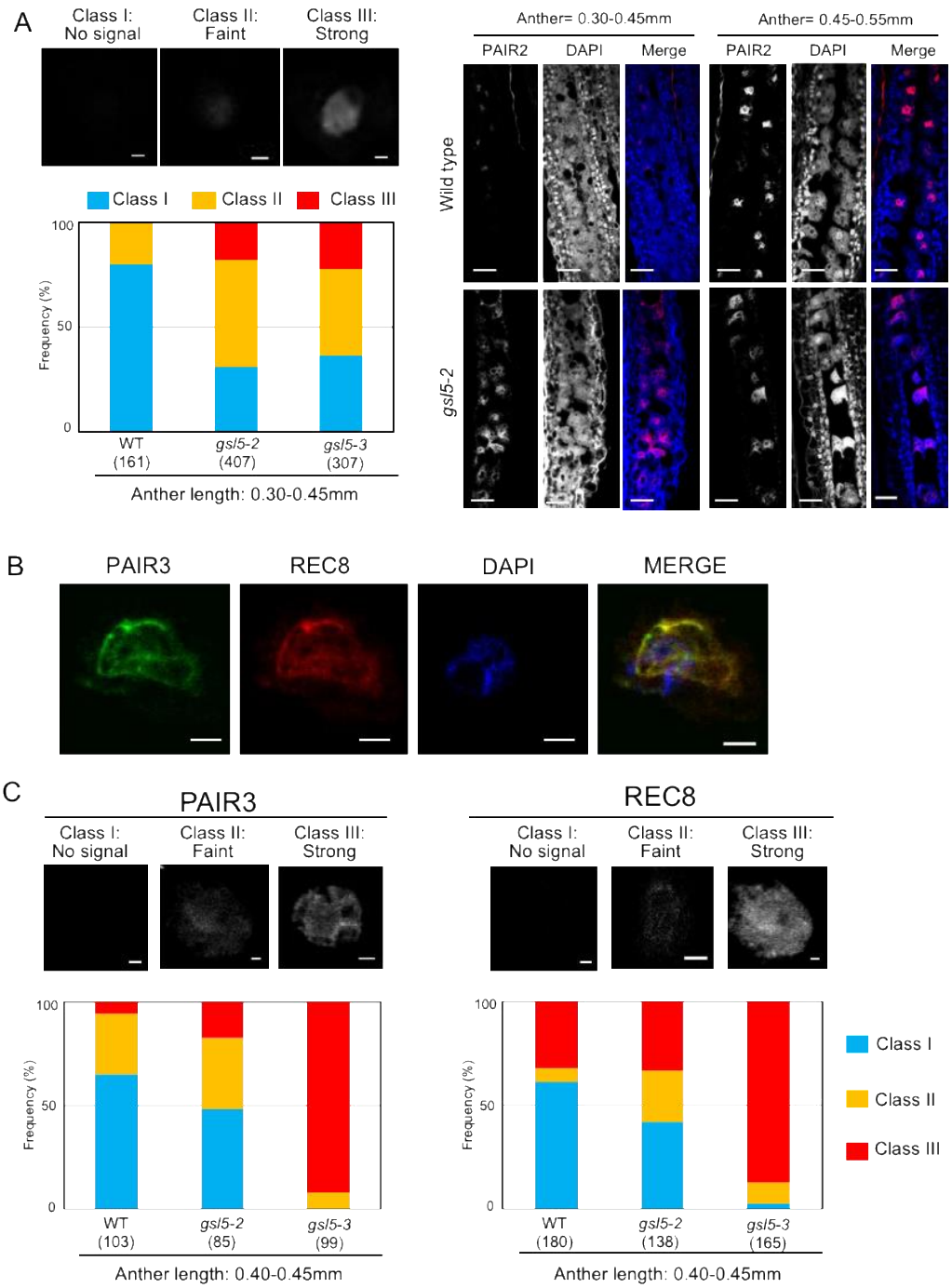

Figure 16. Precocious accumulation of PAIR2, PAIR3 and REC8 in *Osgsl5* Pollen Mother Cell (PMC) nuclei. A: Immunostaining of PAIR2 in isolated premeiotic PMCs. The degree of PAIR2 accumulation in the PMC nucleus was categorized into three classes based on the immunofluorescent intensity (left). Bar=2.5µm. The rate of three PAIR2 classes in each of Wild type (WT), *Osgsl5-2* and *Osgsl5-3* premeiotic anthers (left below). Immunostaining of PAIR2 on longitudinal premeiotic anther sections with anti-PAIR2 antibody. Bar= 50µm. B: Loading of PAIR2 and REC8 onto meiotic chromosomes during zygotene stage in WT, Bar=5µm. C: Immunostaining of PAIR3 (left) and REC8 (right) in the nucleoplasm of isolated premeiotic Pollen Mother Cells (PMC). The degree of PAIR3 and REC8 accumulation in the PMC nucleus was categorized into three classes based on the immunofluorescent intensity, Bar=2.5µm . Below graph represents the quantification of 3 classes of PAIR3 and REC8 signals in each of WT, *Osgsl5-2* and *Osgsl5-3* premeiotic anthers (0.4-0.45mm).

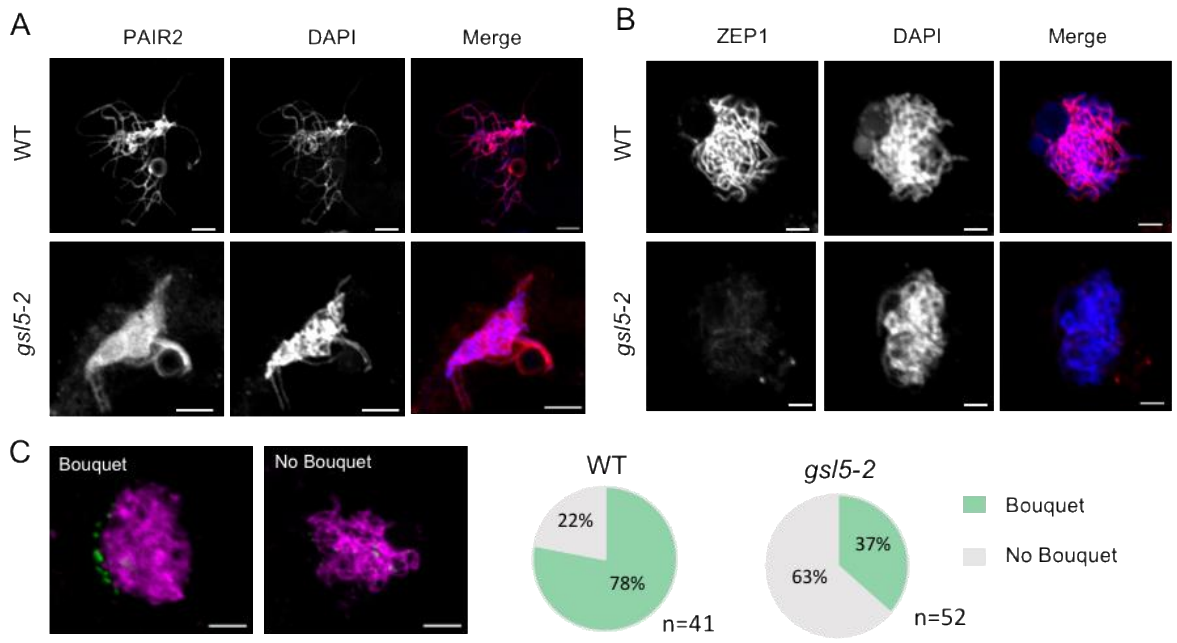

Figure 17. ZEP1 loading to and bouquet frequency of meiotic chromosomes affected, but PAIR2 loading unaffected in *Osgsl5* anthers. A: Immunostaining of PAIR2 in wild type (WT) (n=168) and *Osgsl5-2* (n=134). PAIR2 loading is unaffected in *Osgsl5* mutant. B: Immunostaining of ZEP1 in WT (n=92) and *Osgsl5-2* (n=92). ZEP1 loading onto chromosomes was inhibited in *Osgsl5* mutant. C: Bouquet structures visualized by immunostaining of telomere specific OsPOT1 (green) and DAPI (magenta) during leptotene-zygotene transition (0.50-0.55mm anther) in Pollen Mother Cells of WT (n=41) and *Osgsl5-2* (n=52). Bar=5µm.

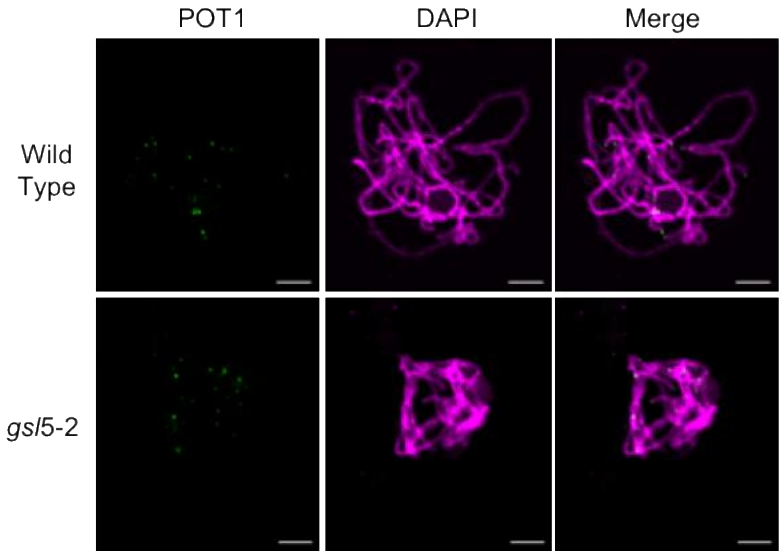

Figure 18. Telomere bouquet structures visualized at late prophase stage. Note that no bouquet was observed both in 0.6-0.7mm WT and *Osgsl5-2* anthers. Bar=5μm.

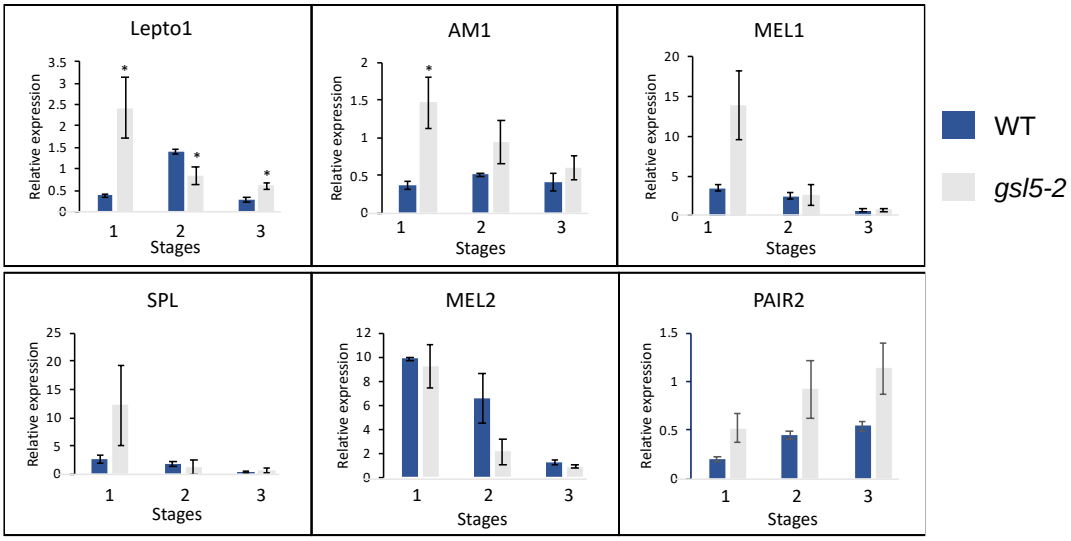

Figure 19. Transcript levels of various genes during mitosis to meiosis transition in wild type (WT) and *Osgsl5-2* anthers. In each panel, 1, 2 and 3 correspond to stages during mitosis-meiosis transition in 0.3-0.4mm, 0.4-0.5mm and 0.5-0.6mm anthers, respectively. Error bars indicate a standard deviation of the mean of three biological replicates. Anthers from >10 florets collected and used in each replicate. Asterisks indicate significant differences *(*P*<0.05 by Student's *t*-test) between WT and *Osgsl5-2.*

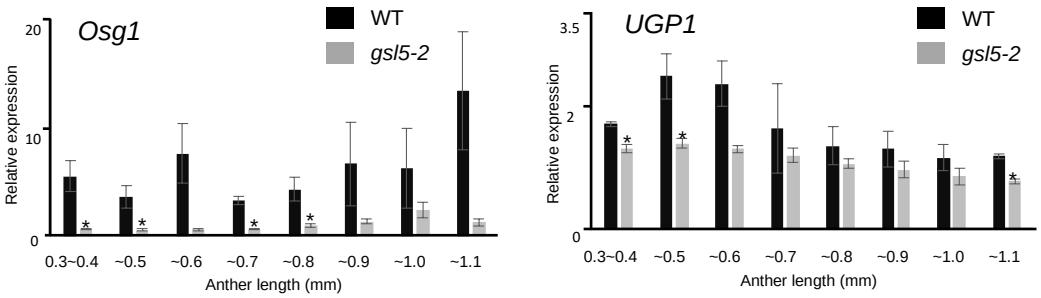

Figure 20. Reduced expression of rice *Osg1* and *UGP1* genes in *Osgsl5-2* anthers. Relative expression levels of callose metabolizing genes, *Osg1* and *UGP1*, in wild type (WT) and *Osgsl5-2* anthers by RT-qPCR. Errors bars indicate standard deviations of means of three biological replicates. Asterisks indicate significant differences *(*P*<0.05 by Student's *t*-test) between WT and *Osgsl5-2.*

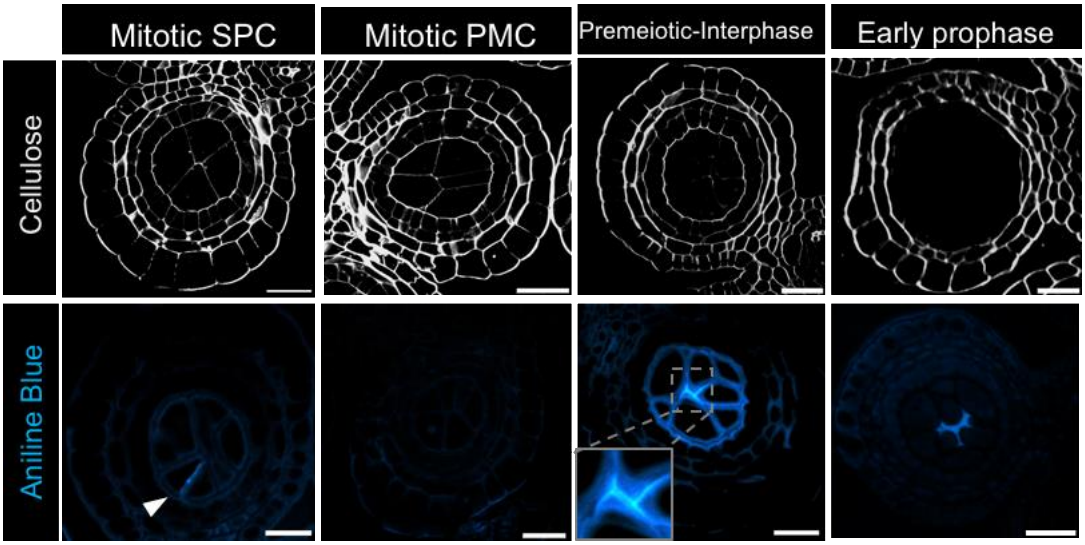

Figure 21. Turnover of cellulose and callose walls during mitosis to meiosis transition period in rice anthers. Above panel shows the staining of cellulosic walls of anther sections with Renaissance 2200. Below panel shows staining of callose walls with aniline blue. During mitotic SPC stage, callose is not detected in anther cells, except on the newly formed cell plate between dividing daughter cells (an arrowhead). Cellulose composing anther-locular cell walls gradually disappear alongside with callose fulfilling intercellular spaces of anther locules around premeiotic interphase. Scale Bar= 20μm.

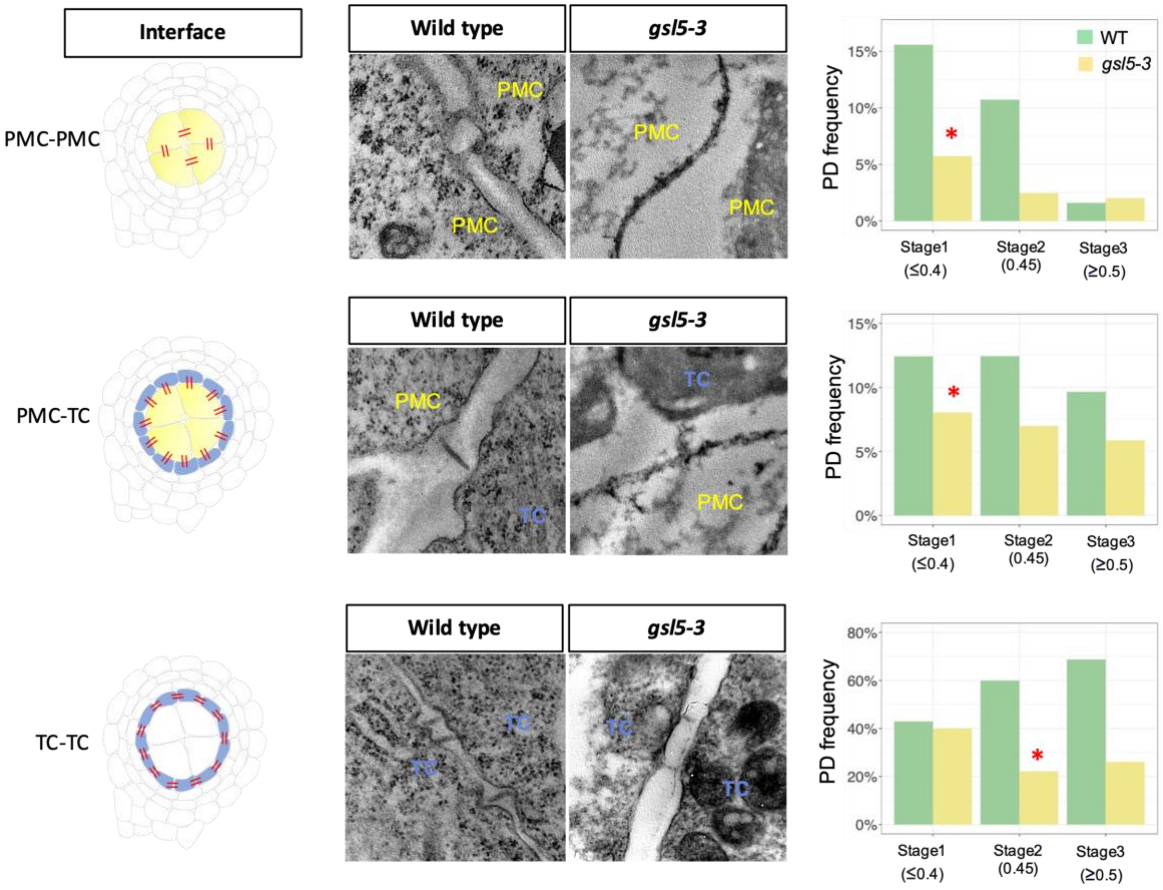

Figure 22: Plasmodesmata frequency reduced in *gsl5-3* mutant anthers. Dynamics of plasmodesmata (PD) observed at three cellular interfaces in anther locules (left). Transmission electron microscopic images showing the distribution of PDs at three cellular interfaces between wild type and *gsl5-3* anthers. Quantification of PD frequency is shown on the right side. Red asterisks indicate significant differences (**P*<0.05 by Student's *t*-test) between WT and *Osgsl5-3.* Anther lengths of respective stages (1,2 and 3) are indicated in the brackets.

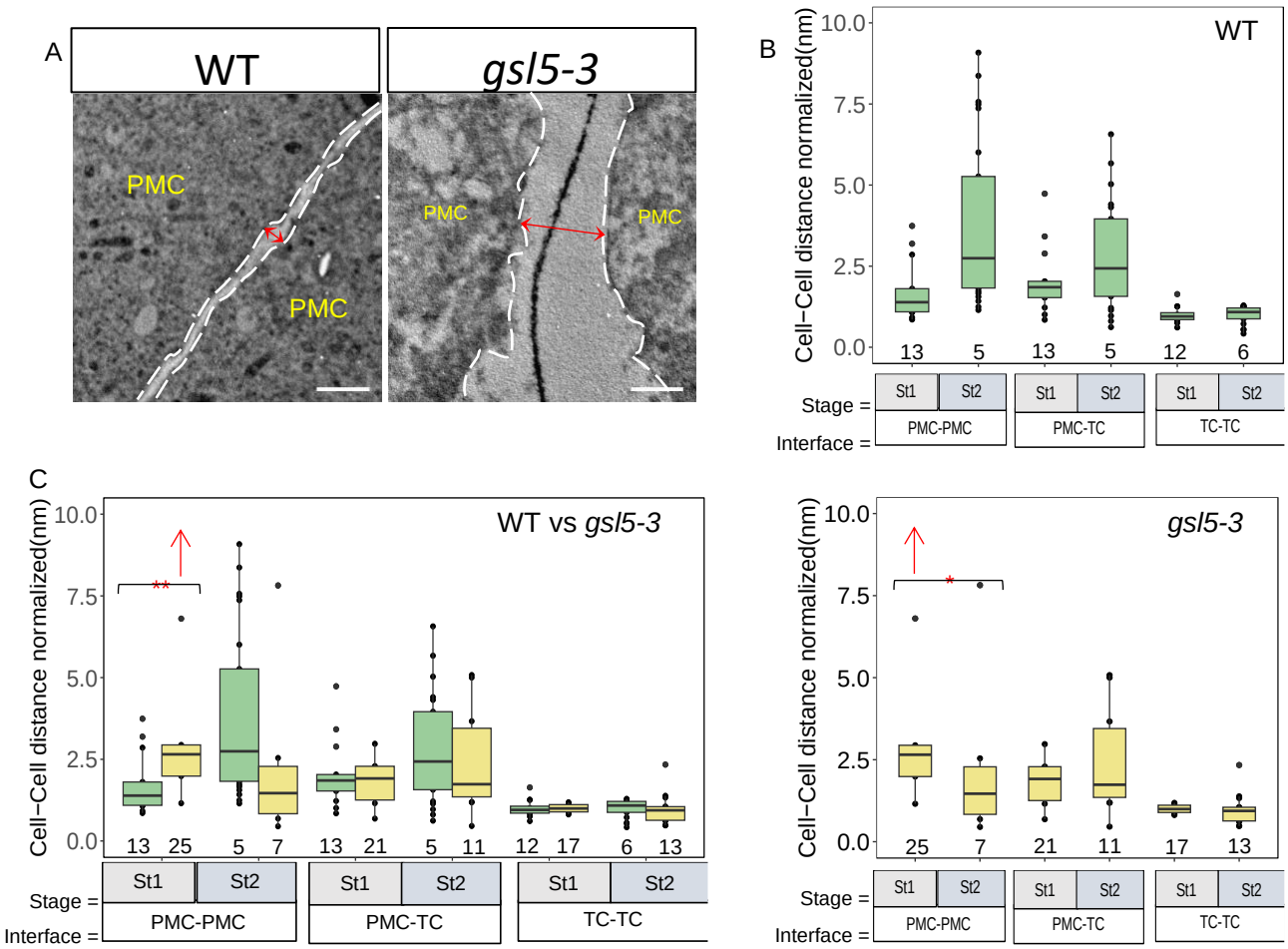

Figure 23: PMC-PMC cell-cell distance greatly increased upon entry into meiosis. A: Representative image showing the apoplast space (red double arrowhead) between PMC-PMC interface. Boundaries of plasma membrane is highlighted by white dashed lines. B: Comparision of cell–cell distance normalized against TC-TC cell distance (nm) in among WT (above) and *gsl5-3* (below) anthers at three cellular interfaces indicated below during mitosis and meiosis stages. C: Comparision of cell–cell distance normalized against TC-TC cell distance (nm) between WT and *gsl5-3* anthers at three cellular interfaces indicated below during mitosis and meiosis stages. Asterisks indicate significant differences (*$p \leq 0.05$, **$p \leq 0.01$, ***$p \leq 0.001$ by Mann Whitney's U Test) between WT and *Osgsl5-3*. Stage1 (St1) anther length = 0.35-0.45mm, Stage2 (St2) anther length = 0.50-0.55mm. Scale = 1um

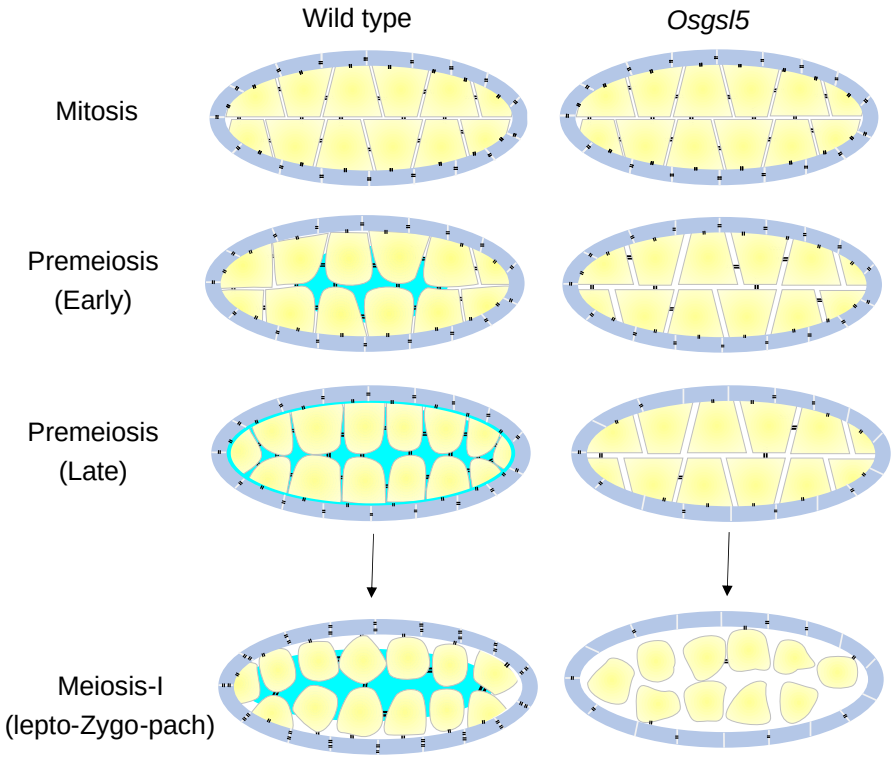

Figure 24. Model showing the action of callose on PMC cell shaping, PD numbers and cell-cell distance during mitosis-meiosis transition in anthers. Notice the changes associated with PMCs (yellow), Tapetal cells (lightsteel blue), Callose (cyan blue) and plasmodesmata connections (double lines) during mitosis-meiosis transition in WT (left) and *gsl5* (right).

Tables

Table 1. Oligo DNA sequences for guide RNA constructions and PCR primers employed in this study.

Primers name	Sequence (5' to 3')	Remarks
CRISPR-gRNAF1	gttgCACTGTGCTGAAATTGGGGG	guide RNA1 sequence used for *gsl5-2* mutant
CRISPR-gRNAR1	aaacCCCCCAATTTCAGCACAGTG	guide RNA1 sequence used for *gsl5-2* mutant
CRISPR-gRNAF2	gttgGCCACAGCTAGGATATATAG	guide RNA2 sequence used for *gsl5-3* mutant
CRISPR-gRNAR2	aaacCTATATATCCTAGCTGTGGC	guide RNA2 sequence used for *gsl5-3* mutant
PU6 gRNA1 Seq	TGCTGGAATTGCCCTTGGATCATGAACCA	To check gRNA1 insertion in PU6
PU6 gRNA2 Seq_1	CATTTTAGACTTTGTTCTGAAC	To check gRNA2 insertion in PU6
PU6 gRNA3 Seq_2	GGAATTTTGCTTCCATTTACTT	To check gRNA2 insertion in PU6
GSL5_2	GCTTCAAGACATGTTAGAAG	gRNA1 genotype sequencing
GSL5_3	GGTCATCATAAATGCAAGTTCCT	gRNA2 genotype sequencing
ISP5 F1	caccTCAGCACAGTGGGATGAGCAGA	GSL5 cDNA cloning for antibody production
ISP5 R2	ctaGTCTTCTATTCAGTTTTGGTA	GSL5 cDNA cloning for antibody production
M13 F	GTAAAACGACGGCCAGT	Universal primer for constructions for sequencing and colony PCR
M13 R	GGAAACAGCTATGACCATG	Universal primer for constructions for sequencing and colony PCR
T7Pro F	TAATACGACTCACTATAGGG	Sequencing of pDEST-ISP5 insertion
POT1F	ccacATGAAAGATCTTGAACTGCAGTTA	POT1 cDNA cloning for antibody production
POT1R	ctaTCAATCCCTGATCTCTGTGCCAA	POT1 cDNA cloning for antibody production
GSP1	GATGAATTTGGGTGGCAATGCGAC	POT1 5' and 3' RACE primer
450	TCCAGATCTCCCGCATCTTG	GSL5_F for RT-PCR
451	GACCTAACCTCTTGTGATGC	GSL5 _R for RT-PCR
549	GTCGTACCACAGGTATTGTG	Actin_F for RT-PCR
550	AGGTAATCAGTGAGAT	Actin_R for RT-PCR
H96	AACTGTCGTGGACCGTCAGA	OsMEL1_F for RT-PCR
H97	GTGGGACCACAGACACTGC	OsMEL1_R for RT-PCR
H135	GCTCCATATCCCAAGAGTGATTAC	OsMEL2_F for RT-PCR
H136	ACGCTCCATGACTCCCACATATT	OsMEL2_R for RT-PCR
H104	CACCTGAGTGGCCATGAAATGAG	OsPAIR2_F for RT-PCR
H105	TTTCTGACCTTCTGCCCGAGAAC	OsPAIR2_R for RT-PCR
H280	ACAGGTGTTATCTATGAAGGACATG	OsAM1_F for RT-PCR
H281	ACCACCATCAACATACAGTGGTT	OsAM1_R for RT-PCR
H282	TAACCAGCTTGGCATCGAGAAGG	OsLEPTO1_F for RT-PCR
H283	AGAATGTTGTTTGCCTGGGTATG	OsLEPTO1_R for RT-PCR
H284	ACCTCTGCTCCAAGACAATG	OsSPL_F for RT-PCR
H285	AAGAACTCGATCTCCCTCACCT	OsSPL_R for RT-PCR
H194	AGGAGGAGTCGATGCCCTCAT	Osg1_F for RT-PCR
H195	GGATGAGAAGCCTCTTCTTGATGG	Osg1_R for RT-PCR
H196	TCTGATTTGTACACCTTGGTCG	UGP1_F for RT-PCR
H197	ATGGTCACCTTACCCTTGAGTG	UGP1_R for RT-PCR
1800	CTCAACTTCCACCTCCTCCA	EAT1_F for RT-PCR
1801	TAGTGGCCGCCGTAGTAGTC	EAT1_R for RT-PCR
1954	AGGGATGATCAAGACAATCAGCTC	TIP2_F for RT-PCR
1955	GATAAAATTCTCTCCAATCCTGGTCA	TIP2_R for RT-PCR

Table 2. Seed setting in Wild type (WT), osgsl5-2 and osgsl5-3						
	Wild Type		*gsl5-2*		*gsl5-3*	
	Fertile seed No.	Total spikelet No.	Fertile seed No.	Total spikelet No.	Fertile seed No.	Total spikelet No.
panicle#1	23	35	0	45	0	32
panicle#2	28	39	0	24	0	25
panicle#3	25	40	0	34	0	17
panicle#4	48	77	0	28	0	39
panicle#5	18	34	0	26	0	22
Total	142	225	0	157	0	135
Fertility (%)	63.1		0.0		0.0	

Table 3. Pollen Mother Cells (PMC) counting data on the basis of Figure 6 graphs.

Table 3-1. No. of PMCs counted in WT anthers.

Anther length (mm)	No. PMCs*																		No. ab-PMCs (%)		Total
	Premei	(%)	Lepto	(%)	Zygo	(%)	Pachy	(%)	Diplo/Diak	(%)	Meta/Telo I	(%)	Dyad	(%)	Tet/MS	(%)					
0.3-0.4	26	(61.9)	16	(38.1)	0	(0.0)	0	(0.0)	0	(0.0)	0	(0.0)	0	(0.0)	0	(0.0)	0	(0.0)	42		
0.4-0.5	14	(9.7)	22	(15.3)	108	(75.0)	0	(0.0)	0	(0.0)	0	(0.0)	0	(0.0)	0	(0.0)	0	(0.0)	144		
0.5-0.6	0	(0.0)	10	(2.3)	67	(15.7)	237	(55.6)	94	(22.1)	18	(4.2)	0	(0.0)	0	(0.0)	0	(0.0)	426		
0.6-0.7	0	(0.0)	0	(0.0)	0	(0.0)	241	(69.3)	87	(25.0)	15	(4.3)	5	(1.4)	0	(0.0)	0	(0.0)	348		
0.7-0.8	0	(0.0)	0	(0.0)	0	(0.0)	18	(13.3)	46	(34.1)	10	(7.4)	26	(19.3)	35	(25.9)	0	(0.0)	135		
0.8-0.9	0	(0.0)	0	(0.0)	0	(0.0)	0	(0.0)	0	(0.0)	0	(0.0)	0	(0.0)	8	(100.0)	0	(0.0)	8		

*: Premei; Premeiosis, Lepto; Leptotene, Zygo; Zygotene, Pachy; Pachytene, Diplo/Diak;, Diplotene/Diakinesis, Meta/Telo I; Metaphase I/Telophase I, Tet/MS; Tetrad/Microspore.

Table 3-2. No. of both wl-PMCs and ab-PMCs counted in gsl5-2 anthers.

Anther length (mm)	No. wl-PMCs																		No. ab-PMCs (%)		Total
	Premei	(%)	Lepto	(%)	Zygo	(%)	Pachy	(%)	Diplo/Diak	(%)	Meta/Telo I	(%)	Dyad	(%)	Tet/MS	(%)					
0.3-0.4	15	(75.0)	5	(25.0)	0	(0.0)	0	(0.0)	0	(0.0)	0	(0.0)	0	(0.0)	0	(0.0)	0	(0.0)	20		
0.4-0.5	3	(1.4)	47	(21.4)	98	(44.5)	28	(12.7)	15	(6.8)	0	(0.0)	0	(0.0)	0	(0.0)	29	(13.2)	220		
0.5-0.6	0	(0.0)	0	(0.0)	93	(44.9)	83	(40.1)	4	(1.9)	4	(1.9)	6	(2.9)	0	(0.0)	17	(8.2)	207		
0.6-0.7	0	(0.0)	0	(0.0)	0	(0.0)	35	(20.2)	46	(26.6)	19	(11.0)	3	(1.7)	0	(0.0)	70	(40.5)	173		
0.7-0.8	0	(0.0)	0	(0.0)	0	(0.0)	14	(10.4)	29	(21.6)	16	(11.9)	8	(6.0)	5	(3.7)	62	(46.3)	134		
0.8-0.9	0	(0.0)	0	(0.0)	0	(0.0)	0	(0.0)	0	(0.0)	0	(0.0)	2	(9.5)	19	(90.5)	0	(0.0)	21		

Table 3-3. No. of both wl-PMCs and ab-PMCs counted in gsl5-3 anthers.

Anther length (mm)	No. wl-PMCs																		No. ab-PMCs (%)		Total
	Premei	(%)	Lepto	(%)	Zygo	(%)	Pachy	(%)	Diplo/Diak	(%)	Meta/Telo I	(%)	Dyad	(%)	Tet/MS	(%)					
0.3-0.4	7	(17.9)	7	(17.9)	16	(41.0)	9	(23.1)	0	(0.0)	0	(0.0)	0	(0.0)	0	(0.0)	0	(0.0)	39		
0.4-0.5	4	(2.9)	24	(17.4)	17	(12.3)	32	(23.2)	32	(23.2)	0	(0.0)	0	(0.0)	0	(0.0)	29	(21.0)	138		
0.5-0.6	0	(0.0)	10	(5.3)	79	(42.0)	91	(48.4)	0	(0.0)	0	(0.0)	8	(4.3)	0	(0.0)	0	(0.0)	188		
0.6-0.7	0	(0.0)	0	(0.0)	9	(7.5)	23	(19.2)	23	(19.2)	29	(24.2)	0	(0.0)	0	(0.0)	36	(30.0)	120		
0.7-0.8	0	(0.0)	0	(0.0)	0	(0.0)	0	(0.0)	15	(15.5)	3	(3.1)	15	(15.5)	35	(36.1)	29	(29.9)	97		
0.8-0.9	0	(0.0)	0	(0.0)	0	(0.0)	0	(0.0)	0	(0.0)	0	(0.0)	0	(0.0)	23	(100.0)	0	(0.0)	23		

Table 3-4. No. of ab-PMCs displaying different chromosomal morphologies in gsl5-2 anthers.

Anther length (mm)	No. ab-PMCs counted*								Total
	Diplo/Diak (%) Agg.**		Diplo/Diak (%) Agg_peri**		Diplo/Diak (%) Uni/Multivalents		Meta/Telo I (%) Uni/Multivalents		
0.3-0.4	0	(0.0)	0	(0.0)	0	(0.0)	0	(0.0)	0
0.4-0.5	18	(62.1)	7	(24.1)	4	(13.8)	0	(0.0)	29
0.5-0.6	2	(11.8)	3	(17.6)	6	(35.3)	6	(35.3)	17
0.6-0.7	28	(40.0)	23	(32.9)	12	(17.1)	7	(10.0)	70
0.7-0.8	31	(50.0)	20	(32.3)	7	(11.3)	4	(6.5)	62
0.8-0.9	0	(0.0)	0	(0.0)	0	(0.0)	0	(0.0)	0

*; Meiotic stages of ab-PMCs were referred to the stages observed in wl-PMCs concomitantly segregated with ab-PMCs

**; Agg.; Aggregated chromosomes, Agg_peri; Aggregated chromosomes located at cell peripheral region

Table 3-5. No. of ab-PMCs displaying different chromosomal morphologies in gsl5-3 anthers.

Anther length (mm)	No. ab-PMCs counted*								Total
	Diplo/Diak (%) Agg.**		Diplo/Diak (%) Agg_peri**		Diplo/Diak (%) Uni/Multivalents		Meta/Telo I (%) Uni/Multivalents		
0.3-0.4	0	(0.0)	0	(0.0)	0	(0.0)	0	(0.0)	0
0.4-0.5	25	(86.2)	4	(13.8)	0	(0.0)	0	(0.0)	29
0.5-0.6	0	(0.0)	0	(0.0)	0	(0.0)	0	(0.0)	0
0.6-0.7	10	(27.8)	12	(33.3)	7	(19.4)	7	(19.4)	36
0.7-0.8	16	(55.2)	12	(41.4)	1	(3.4)	0	(0.0)	29
0.8-0.9	0	(0.0)	0	(0.0)	0	(0.0)	0	(0.0)	0

*; Meiotic stages of ab-PMCs were referred to the stages observed in wl-PMCs concomitantly segregated with ab-PMCs

**; Agg.; Aggregated chromosomes, Agg_peri; Aggregated chromosomes located at cell peripheral region

Table. 4	Gene accession numbers used in this study
GENE ID	Accession number
GSL5	XM_015788415.2
MEL1	XM_015773749.2
MEL2	HM047138.1
PAIR2	NM_001403897.1
PAIR3	XM_015759397.2
REC8	XM_015782607.2
EAT1	XM_015779154.2
TIP2	NM_001409411.1
ZEP1	XM_015779028.2
SPL	XM_015783619.2
LEPTO1	BR000253.1
AM1	XM_015775894.2
OSG1	XM_015795591.2
UGP1	XM_015756425.2
RBOHF	AP014964.1

References

Abou-Saleh, R.H., M.C. Hernandez-Gomez, S. Amsbury, C. Paniagua, M. Bourdon, S. Miyashima, Y. Helariutta, M. Fuller, T. Budtova, and Connell SD. 'Interactions between Callose and Cellulose Revealed through the Analysis of Biopolymer Mixtures'. *Nature Communications* 9, no. 1 (2018): 4538. https://doi.org/10.1038/s41467-018-06820-y.

Albert, B., A. Ressayre, and S. Nadot. 'Correlation between Pollen Aperture Pattern and Callose Deposition in Late Tetrad Stage in Three Species Producing Atypical Pollen Grains'. *American Journal of Botany* 98, no. 2 (2011): 189–96. https://doi.org/10.3732/ajb.1000195.

An, Q., R. Hückelhoven, K.H. Kogel, and A.J. Bel. 'Multivesicular Bodies Participate in a Cell Wall-Associated Defence Response in Barley Leaves Attacked by the Pathogenic Powdery Mildew Fungus'. *Cell Microbiol* 8, no. 6 (2006): 1009–19. https://doi.org/10.1111/j.1462-5822.2006.00683.x.

Bachelier, J.B., and W.E. Friedman. 'Female gamete Zcompetition in an ancient angiosperm lineage. Proc Natl Acad Sci U S A'. *Epub* 26;108(30):12360-5 (July 2011). https://doi.org/10.1073/pnas.1104697108.

Barnett, JR. 'Plasmodesmata and pit development in secondary xylem elements'. *Planta* 155, no. 3 (1982): 251–60. https://doi.org/10.1007/BF00392724.

Beebe, Dwight U., and Ray F. Evert. 'Photoassimilate Pathway(s) and Phloem Loading in the Leaf of Moricandia Arvensis (L.) DC'. *Brassicaceae)." International Journal of Plant Sciences* 153, no. 1 (1992): 61–77.

Benitez-Alfonso, Y., D. Jackson, and A. Maule. 'Redox Regulation of Intercellular Transport'. *Protoplasma* Jan;248(1):131-40 (2011). https://doi.org/10.1007/s00709-010-0243-4.

Bhalla, P.L., and H.D. Slattery. 'Callose Deposits Make Clover Seeds Impermeable to Water'. *Annals of Botany* 53, no. 1 (1984): 125–28. https://doi.org/10.1093/oxfordjournals.aob.a086661.

Chen, R., X. Zhao, Z. Shao, Z. Wei, Y. Wang, L. Zhu, J. Zhao, M. Sun, R. He, and G. He. 'Rice UDP-Glucose Pyrophosphorylase1 Is Essential for Pollen Callose Deposition and Its Cosuppression

Results in a New Type of Thermosensitive Genic Male Sterility'. *The Plant Cell* 19, no. 3 (2007): 847–61. https://doi.org/10.1105/tpc.106.044123.

Chen, X.Y., and J.Y. Kim. 'Callose Synthesis in Higher Plants'. *Plant Signaling & Behavior* 4, no. 6 (2009): 489–92. https://doi.org/10.4161/psb.4.6.8359.

Dong, X., Z. Hong, J. Chatterjee, S. Kim, and D.P.S. Verma. 'Expression of Callose Synthase Genes and Its Connection with Npr1 Signaling Pathway during Pathogen Infection'. *Planta* 229, no. 1 (2008): 87–98. https://doi.org/10.1007/s00425-008-0812-3.

Dong, X., Z. Hong, M. Sivaramakrishnan, M. Mahfouz, and D.P. Verma. 'Callose Synthase (CalS5) Is Required for Exine Formation during Microgametogenesis and for Pollen Viability in Arabidopsis'. *The Plant Journal : For Cell and Molecular Biology* 42, no. 3 (2005): 315–28. https://doi.org/10.1111/j.1365-313X.2005.02379.x.

Eggert, D., M. Naumann, and R. Reimer. 'Nanoscale Glucan Polymer Network Causes Pathogen Resistance'. *Sci Rep* 4, no. 4159 (2014). https://doi.org/10.1038/srep04159.

Frankel, R., S. Izhar, and J. Nitsan. 'Timing of callase activity and cytoplasmic male sterility in Petunia'. *Biochemical Genetics* 3, no. 5 (1969): 451–55. https://doi.org/10.1007/BF00485605.

Franklin-Tong, V.E. 'Signaling and the Modulation of Pollen Tube Growth'. *The Plant Cell* 11, no. 4 (1999): 727–38. https://doi.org/10.1105/tpc.11.4.727.

Fu, Z., J. Yu, X. Cheng, X. Zong, J. Xu, M. Chen, Z. Li, D. Zhang, and W. Liang. 'The Rice Basic Helix-Loop-Helix Transcription Factor TDR INTERACTING PROTEIN2 Is a Central Switch in Early Anther Development'. *The Plant Cell* 26, no. 4 (2014): 1512–24. https://doi.org/10.1105/tpc.114.123745.

Goldberg, R.B., T.P. Beals, and P.M. Sanders. 'Anther Development: Basic Principles and Practical Applications'. *Plant Cell* Oct;5(10):1217-29 (1993). https://doi.org/10.1105/tpc.5.10.1217.

Harada, T., A. Misaki, and H. Saito. 'Curdlan: A Bacterial Gel-Forming Beta-1,3-Glucan'. *Arch Biochem Biophys* 124, no. 1 (1968): 292–98. https://doi.org/10.1016/0003-9861(68)90330-5.

Hartwell, L.H. 'Saccharomyces Cerevisiae Cell Cycle'. *Bacteriol Rev* Jun;38(2):164-98 (1974). https://doi.org/10.1128/br.38.2.164-198.1974.

Heslop-harrison, J. ‘Cell Walls, Cell Membranes and Protoplasmic Connections during Meiosis and Pollen Development’. Edited by H.F. Linskens. Amsterdam: North Holland Publishers, 1964.

Hiei, Y., S. Ohta, T. Komari, and T. Kumashiro. ‘Efficient TranFig Sormation of Rice (Oryza Sativa L.) Mediated by Agrobacterium and Sequence Analysis of the Boundaries of the T-DNA’. *The Plant Journal : For Cell and Molecular Biology* 6, no. 2 (1994): 271–82. https://doi.org/10.1046/j.1365-313x.1994.6020271.x.

Higgins, J.D., R.M. Perry, A. Barakate, L. Ramsay, R. Waugh, C. Halpin, S.J. Armstrong, and C.H. Franklin. ‘Spatiotemporal Asymmetry of the Meiotic Program Underlies the Predominantly Distal Distribution of Meiotic Crossovers in Barley’. *Plant Cell* 24, no. 10 (2012): 4096–4109. https://doi.org/10.1105/tpc.112.102483.

Hill, N.S., R. Kadoya, D.K. Chattoraj, and P.A. Levin. ‘Cell Size and the Initiation of DNA Replication in Bacteria’. *PLoS Genet* 8, no. 3 (2012). https://doi.org/10.1371/journal.pgen.1002549.

Hong, Z., A.J. Delauney, and D.P. Verma. ‘A Cell Plate-Specific Callose Synthase and Its Interaction with Phragmoplastin’. *The Plant Cell* 13, no. 4 (2001): 755–68. https://doi.org/10.1105/tpc.13.4.755.

Hu, L., W. Liang, C. Yin, X. Cui, J. Zong, X. Wang, J. Hu, and D. Zhang. ‘Rice MADS3 Regulates ROS Homeostasis during Late Anther Development’. *Plant Cell* Feb;23(2):515-33 (2011). https://doi.org/10.1105/tpc.110.074369.

Huang, H., F. Ullah, D.X. Zhou, M. Yi, and Y. Zhao. ‘Mechanisms of ROS Regulation of Plant Development and Stress Responses’. *Front Plant Sci. Jun* 10, no. 800 (2019). https://doi.org/10.3389/fpls.2019.00800.

Huang, J., C. Wang, H. Wang, P. Lu, B. Zheng, H. Ma, G.P. Copenhaver, and Y. Wang. ‘Meiocyte-Specific and AtSPO11-1-Dependent Small RNAs and Their Association with Meiotic Gene Expression and Recombination’. *The Plant Cell* 31, no. 2 (2019): 444–64. https://doi.org/10.1105/tpc.18.00511.

Iannone, M.F., E.P. Rosales, M.D. Groppa, and M.P. Benavides. ‘Reactive Oxygen Species Formation and Cell Death in Catalase-Deficient Tobacco Leaf Disks Exposed to Cadmium’. *Protoplasma* 245, no. 1–4 (2010): 15–27.

Itoh, J., K.I. Nonomura, K. Ikeda, S. Yamaki, Y. Inukai, H. Yamagishi, H. Kitano, and Y. Nagato.

‘Rice plant development: from zygote to spikelet’. *Plant & cell physiology* 46, no. 1 (2005): 23–47. https://doi.org/10.1093/pcp/pci501.

Jacobs, A.K., V. Lipka, R.A. Burton, R. Panstruga, N. Strizhov, P. Schulze-Lefert, and G.B. Fincher. ‘An Arabidopsis Callose Synthase, GSL5, Is Required for Wound and Papillary Callose Formation’. *The Plant Cell* 15, no. 11 (2003): 2503–13. https://doi.org/10.1105/tpc.016097.

Kelliher, T., and V. Walbot. ‘Emergence and Patterning of the Five Cell Types of the Zea Mays Anther Locule’. *Dev Biol* 1;350(1):32-49 (February 2011). https://doi.org/10.1016/j.ydbio.2010.11.005.

Lee, D.K., and L.E. Sieburth. ‘Plasmodesmata Formation: Poking Holes in Walls with Ise’. *Current Biology* 20, no. 11 (2010): 488–90. https://doi.org/10.1016/j.cub.2010.03.047.

Lei, X., and B. Liu. ‘Tapetum-Dependent Male Meiosis Progression in Plants: Increasing Evidence Emerges’. *Frontiers in Plant Science* 10 (2020): 1667. https://doi.org/10.3389/fpls.2019.01667.

Lennon, A.M., U.H. Neuenschwander, M. Ribas-Carbo, L. Giles, and J.A. Ryals. ‘Siedow JN 1997.The Effects of Salicylic Acid and Tobacco Mosaic Virus Infection on the Alternative Oxidase of Tobacco’. *Plant Physiol* 115, no. 2 (n.d.): 783–91.

Libuda, D.E., S. Uzawa, B.J. Meyer, and A.M. Villeneuve. ‘Meiotic Chromosome Structures Constrain and Respond to Designation of Crossover Sites’. *Nature* 31;502(7473):703-6 (October 2013). https://doi.org/10.1038/nature12577.

Liu, B., N. Storme, and D. Geelen. ‘Gibberellin Induces Diploid Pollen Formation by Interfering with Meiotic Cytokinesis’. *Plant Physiology* 173, no. 1 (2017): 338–53. https://doi.org/10.1104/pp.16.00480.

Liu, H., Y. Ding, Y. Zhou, W. Jin, K. Xie, and L.L. Chen. ‘CRISPR-P 2.0: An Improved CRISPR/Cas9 Tool for Genome Editing in Plants’. *Mo Plant* 10, no. 3 (2017): 530–32. https://doi.org/10.1016/j.molp.2017.01.003.

Lucas, W.J., B.K. Ham, and J.Y. Kim. ‘Plasmodesmata - Bridging the Gap between Neighboring Plant Cells’. *Trends in Cell Biology* 19, no. 10 (2009): 495–503. https://doi.org/10.1016/j.tcb.2009.07.003.

Lundgren, K., N. Walworth, R. Booher, M. Dembski, M. Kirschner, and D. Beach. ‘Mik1 and Wee1 Cooperate in the Inhibitory Tyrosine Phosphorylation of Cdc2’. *Cell* 64 (1991): 1111-1122 10

1016 0092-8674 91 90266-2.

Maltby, D., N.C. Carpita, D. Montezinos, C. Kulow, and D.P. Delmer. 'B-1,3-Glucan in Developing Cotton Fibers: Structure, Localization, and Relationship of Synthesis to That of Secondary Wall Cellulose'. *Plant Physiology* 63, no. 6 (1979): 1158–64. https://doi.org/10.1104/pp.63.6.1158.

Mamun, E.A., L.C. Cantrill, R.L. Overall, and B.G. Sutton. 'Cellular Organisation in Meiotic and Early Post-Meiotic Rice Anthers'. *Cell Biology International* 29, no. 11 (2005): 903–13. https://doi.org/10.1016/j.cellbi.2005.08.001.

Manna, M., V.M.M. Achary, and M.K. Reddy. 'ROS Signaling and Its Role in Plants'. In *Sensory Biology of Plants*, edited by S. Sopory. Singapore: Springer, 2019. https://doi.org/10.1007/978-981-13-8922-1_14.

Mikami, M., S. Toki, and M. Endo. 'Comparison of CRISPR/Cas9 Expression Constructs for Efficient Targeted Mutagenesis in Rice'. *Plant Molecular Biology* 88, no. 6 (2015): 561–72. https://doi.org/10.1007/s11103-015-0342-x.

Miyao, A., K. Tanaka, K. Murata, H. Sawaki, S. Takeda, K. Abe, Y. Shinozuka, K. Onosato, and H. Hirochika. 'Target Site Specificity of the Tos17 Retrotransposon Shows a Preference for Insertion within Genes and against Insertion in Retrotransposon-Rich Regions of the Genome'. *Plant Cell* Aug;15(8):1771-80 (2003). https://doi.org/10.1105/tpc.012559.

Murakami, H., and S. Keeney. 'Temporospatial Coordination of Meiotic DNA Replication and Recombination via DDK Recruitment to Replisomes'. *Cell* 158, no. 4 (2014): 861–73. https://doi.org/10.1016/j.cell.2014.06.028.

Mursalimov, Baiborodin, SR, Sidorchuk SI, Shumny YV, Deineko VK, and E.V. 'Characteristics of the Cytomictic Channel Formation in Nicotiana Tabacum L. Pollen Mother Cells'. *Cytology and Genetics* 44, no. 1 (2010): 14–18. https://doi.org/10.3103/S0095452710010032.

Mursalimov, Sidorchuk, SR, Deineko YV, and E.V. 'New Insights into Cytomixis: Specific Cellular Features and Prevalence in Higher Plants'. *Planta* 238, no. 3 (2013): 415–23. https://doi.org/10.1007/s00425-013-1914-0.

Musiał, K., and M. Kościńska-Pająk. 'Pattern of Callose Deposition during the Course of Meiotic Diplospory in Chondrilla Juncea (Asteraceae, Cichorioideae'. *Protoplasma* 254, no. 4 (2017): 1499–1505. https://doi.org/10.1007/s00709-016-1039-y.

Nedukha, O.M. ‘Callose: Localization, Functions, and Synthesis in Plant Cells’. *Cytology and Genetics* 49, no. 1 (2015): 49–57. https://doi.org/10.3103/S0095452715010090.

Niu, N., W. Liang, X. Yang, Weilin Jin, Zoe A. Wilson, Jianping Hu, and Dabing Zhang. ‘EAT1 Promotes Tapetal Cell Death by Regulating Aspartic Proteases during Male Reproductive Development in Rice’. *Nat Commun* 4 (2013): 1445. https://doi.org/10.1038/ncomms2396.

Nonomura, K.I., M. Eiguchi, M. Nakano, K. Takashima, N. Komeda, S. Fukuchi, S. Miyazaki, A. Miyao, H. Hirochika, and N. Kurata. ‘A Novel RNA-Recognition-Motif Protein Is Required for Premeiotic G1/S-Phase Transition in Rice (Oryza Sativa L’. *PLoS Genetics* 7, no. 1 (2011): 1001265. https://doi.org/10.1371/journal.pgen.1001265.

Nonomura, K.I., M. Nakano, M. Eiguchi, T. Suzuki, and N. Kurata. ‘PAIR2 is essential for homologous chromosome synapsis in rice meiosis I’. *Journal of cell science* 119, no. Pt 2 (2006): 217–25. https://doi.org/10.1242/jcs.02736.

Nurse, P. ‘Genetic control of cell size at cell division in yeast’. *Nature* 14;256(5518):547-51 (August 1975). https://doi.org/10.1038/256547a0.

Ono, S., H. Liu, K. Tsuda, E. Fukai, K. Tanaka, T. Sasaki, and K.I. Nonomura. ‘EAT1 Transcription Factor, a Non-Cell-Autonomous Regulator of Pollen Production, Activates Meiotic Small RNA Biogenesis in Rice Anther Tapetum’. *PLoS Genetics* 14, no. 2 (2018): 1007238. https://doi.org/10.1371/journal.pgen.1007238.

Ouedraogo, I., M. Lartaud, C. Baroux, G. Mosca, L. Delgado, O. Leblanc, J.L. Verdeil, G. Conéjéro, and D. Autran. ‘3D cellular morphometrics of ovule primordium development in Zea mays reveal differential division and growth dynamics specifying megaspore mother cell singleness’. *Front Plant Sci*, 12 May 2023. https://doi.org/10.3389/fpls.2023.1174171.

Overmyer, K., M. Brosche, and J. Kangasjarvi. ‘Reactive Oxygen Species and Hormonal Control of Cell Death’. *Trends Plant Sci* 8, no. 7 (2003): 335–42.

Piršelová, B., and I. Matušíková. ‘Callose: The Plant Cell Wall Polysaccharide with Multiple Biological Functions’. *Acta Physiologiae Plantarum* 35, no. 3 (2013): 635–44. https://doi.org/10.1007/s11738-012-1103-y.

Plackett, A., A.C. Ferguson, S.J. Powers, A. Wanchoo-Kohli, A.L. Phillips, Z.A. Wilson, P. Hedden, and S.G. Thomas. ‘DELLA Activity Is Required for Succesful Pollen Development in the

Columbia Ecotype of Arabidopsis'. *The New Phytologist* 201, no. 3 (2014): 825–36. https://doi.org/10.1111/nph.12571.

Pratto, F., K. Brick, G. Cheng, K.G. Lam, J.M. Cloutier, D. Dahiya, Jordan Wellard SR, Camerini-Otero PW, and R.D. 'Meiotic Recombination Mirrors Patterns of Germline Replication in Mice and Humans'. *Cell* 184, no. 16 (2021): 4251–67. https://doi.org/10.1016/j.cell.2021.06.025.

Prieu, C., H. Sauquet, P.H. Gouyon, and B. Albert. 'More than Sixty Origins of Pantoporate Pollen in Angiosperms'. *American Journal of Botany* 104, no. 12 (2017): 1837–45. https://doi.org/10.3732/ajb.1700289.

Qin, P., D. Ting, A. Shieh, and S. McCormick. 'Callose Plug Deposition Patterns Vary in Pollen Tubes of Arabidopsis Thaliana Ecotypes and Tomato Species'. *BMC Plant Biology* 12 (2012): 178. https://doi.org/10.1186/1471-2229-12-178.

Radford, J.E., M. Vesk, and R.L. Overall. 'Callose deposition at plasmodesmata', 1998. *Protoplasma* 201, no. 1–2 (n.d.): 30–37. https://doi.org/10.1007/BF01280708.

Radice, S., M. Ontivero, E. Giordani, and E. Bellini. 'Anatomical differences on development of fertile and sterile pollen grains of Prunus salicina Lindl'. *Plant Systematics and Evolution* 273, no. 1–2 (2008): 63–69. https://doi.org/10.1007/s00606-008-0011-5.

Rodriguez-Serrano, M., M.C. Romero-Puertas, D.M. Pazmino, P.S. Testillano, M.C. Risueno, L.A. Del Rio, and L.M. Sandalio. 'Cellular Response of Pea Plants to Cadmium Toxicity: Cross Talk between Reactive Oxygen Species, Nitric Oxide, and Calcium'. *Plant Physiol* 150, no. 1 (2009): 229–43.

Roschzttardtz, H., G. Conéjéro, F. Divol, C. Alcon, J.L. Verdeil, C. Curie, and S. Mari. 'New insights into Fe localization in plant tissues'. *Frontiers in plant science* 4 (2013): 350. https://doi.org/10.3389/fpls.2013.00350.

Russell, P., and P. Nurse. 'Negative Regulation of Mitosis by Wee1+, a Gene Encoding a Protein Kinase Homolog'. *Cell*, 22 May 1987. https://doi.org/10.1016/0092-8674(87)90458-2.

Sager, R.E., and J.Y. Lee. 'Plasmodesmata at a glance'. *Journal of cell science* 131, no. 11 (2018): 209346. https://doi.org/10.1242/jcs.209346.

Saitô, H., T. Ohki, and T. Sasaki. 'A 13C Nuclear Magnetic Resonance Study of Gel-Forming (1 Goes

to 3)-Beta-d-Glucans. Evidence of the Presence of Single-Helical Conformation in a Resilient Gel of a Curdlan-Type Polysaccharide 13140 from Alcaligenes Faecalis Var. Myxogenes IFO 13140'. *Biochemistry* 16, no. 5 (1977): 908–14. https://doi.org/10.1021/bi00624a015.

Sankaranarayanan, S., Y. Ju, and S.A. Kessler. 'Reactive Oxygen Species as Mediators of Gametophyte Development and Double Fertilization in Flowering Plants'. *Frontiers in Plant Science* 11 (2020): 1199. https://doi.org/10.3389/fpls.2020.01199.

Scott, R.J., M. Spielman, and H.G. Dickinson. 'Stamen Structure and Function'. *The Plant Cell* 16, no. ue suppl_1 (2004). https://doi.org/10.1105/tpc.017012.

Seale, M. 'Callose Deposition during Pollen Development'. *Plant Physiology* 184, no. 2 (2020): 564–65. https://doi.org/10.1104/pp.20.01143.

Sedeek, M., R. Nasrallah, R.M. Touyz, and R.L. Hébert. 'NADPH Oxidases, Reactive Oxygen Species, and the Kidney: Friend and Foe'. *Journal of the American Society of Nephrology : JASN* 24, no. 10 (2013): 1512–18. https://doi.org/10.1681/ASN.2012111112.

Shakirov, E.V., Y.V. Surovtseva, N. Osbun, and D.E. Shippen. 'The Arabidopsis Pot1 and Pot2 Proteins Function in Telomere Length Homeostasis and Chromosome End Protection'. *Molecular and Cellular Biology* 25, no. 17 (2005): 7725–33. https://doi.org/10.1128/MCB.25.17.7725-7733.2005.

Shao, T., D. Tang, K. Wang, M. Wang, L. Che, B. Qin, H. Yu, M. Li, M. Gu, and Z. Cheng. 'OsREC8 is essential for chromatid cohesion and metaphase I monopolar orientation in rice meiosis'. *Plant physiology* 156, no. 3 (2011): 1386–96. https://doi.org/10.1104/pp.111.177428.

Shi, X., X. Sun, Z. Zhang, D. Feng, Q. Zhang, L. Han, J. Wu, and T. Lu. 'GLUCAN SYNTHASE-LIKE 5 (GSL5) Plays an Essential Role in Male Fertility by Regulating Callose Metabolism during Microsporogenesis in Rice'. *Plant & Cell Physiology* 56, no. 3 (2015): 497–509. https://doi.org/10.1093/pcp/pcu193.

Shivanna, K.R. *Pollen Biology and Biotechnology*. Science Publishers. Plymouth, 2003.

Song, L., R. Wang, L. Zhang, Y. Wang, and S. Yao. 'CRR1 Encoding Callose Synthase Functions in Ovary Expansion by Affecting Vascular Cell Patterning in Rice'. *The Plant Journal : For Cell and Molecular Biology* 88, no. 4 (2016): 620–32. https://doi.org/10.1111/tpj.13287.

Staehelin LA., and Hepler PK. 'Cytokinesis in Higher Plants'. *Cell* 84, no. 6 (1996): 821–24. https://doi.org/10.1016/s0092-8674(00)81060-0.

Steer, M.W. 'Differentiation of the tapetum in Avena. I. The cell surface'. *Journal of cell science* 25 (1977): 125–38. https://doi.org/10.1242/jcs.25.1.125.

Stieglitz, H., and H. Stern. 'Regulation of β-1,3-Glucanase Activity in Developing Anthers of Lilium'. *Dev. Biol* 34 (1973): 169–73. https://doi.org/10.1016/0012-1606(73)90347-3.

Stone, B.A., and A.E. Clarke. *Chemistry and Biology of (1-3)-β-D-Glucans*. La Trobe University Press, 1992.

Thiele, K., G. Wanner, V. Kindzierski, G. Jürgens, U. Mayer, F. Pachl, and F.F. Assaad. 'The Timely Deposition of Callose Is Essential for Cytokinesis in Arabidopsis'. *The Plant Journal* 58 (2009): 13–26. https://doi.org/10.1111/j.1365-313X.2008.03760.x.

Tripathy, B.C., and R. Oelmüller. 'Reactive Oxygen Species Generation and Signaling in Plants'. *Plant Signaling & Behavior* 7, no. 12 (2012): 1621–33. https://doi.org/10.4161/psb.22455.

Tsuda, K., and G. Chuck. *Heat Induced Epitope Retrieval (HIER) Assisted Protein Immunostaining in Maize*. Bio-101: e3260, 2019. https://doi.org/10.21769/BioProtoc.3260.

Tucker, M.R., and A.M. Koltunow. 'Traffic Monitors at the Cell Periphery: The Role of Cell Walls during Early Female Reproductive Cell Differentiation in Plants'. *Curr Opin Plant Biol* 17 (2014): 137–45. https://doi.org/10.1016/j.pbi.2013.11.015.

Unal, M., F. Vardar, and Ayturk zlem. 'Callose in Plant Sexual Reproduction'. In *Current Progress in Biological Research. InTech*, edited by M. Silva-Opps, 2013. https://doi.org/10.5772/53001.

Voelkel-Meiman, K., S.Y. Cheng, S.J. Morehouse, and A.J. MacQueen. 'Synaptonemal Complex Proteins of Budding Yeast Define Reciprocal Roles in MutSγ-Mediated Crossover Formation'. *Genetics* Jul;203(3):1091-103 (2016). https://doi.org/10.1534/genetics.115.182923.

Voigt, C.A. 'Callose-Mediated Resistance to Pathogenic Intruders in Plant Defense-Related Papillae'. *Frontiers in Plant Science* 5 (2014): 168. https://doi.org/10.3389/fpls.2014.00168.

Wan, L., W. Zha, X. Cheng, C. Liu, L. Lv, C. Liu, Z. Wang, et al. 'A rice β-1,3-glucanase gene Osg1 is required for callose degradation in pollen development'. *Planta* 233, no. 2 (2011): 309–23.

https://doi.org/10.1007/s00425-010-1301-z.

Wang, K., C. Wang, Q. Liu, W. Liu, and Y. Fu. 'Increasing the Genetic Recombination Frequency by Partial Loss of Function of the Synaptonemal Complex in Rice'. *Mol Plant* 8, no. 8 (2015): 1295–98. https://doi.org/10.1016/j.molp.2015.04.011.

Wang, K., M. Wang, D. Tang, Y. Shen, B. Qin, M. Li, and Z. Cheng. 'PAIR3, an Axis-Associated Protein, Is Essential for the Recruitment of Recombination Elements onto Meiotic Chromosomes in Rice'. *Molecular Biology of the Cell* 22, no. 1 (2011): 12–19. https://doi.org/10.1091/mbc.E10-08-0667.

Wang, M., K. Wang, D. Tang, C. Wei, M. Li, Y. Shen, Z. Chi, M. Gu, and Z. Cheng. 'The Central Element Protein ZEP1 of the Synaptonemal Complex Regulates the Number of Crossovers during Meiosis in Rice'. *The Plant Cell* 22, no. 2 (2010): 417–30. https://doi.org/10.1105/tpc.109.070789.

Watanabe, N., M. Broome, and T. Hunter. 'Regulation of the Human WEE1Hu CDK Tyrosine 15-Kinase during the Cell Cycle'. *EMBO J* 14, no. 9 (1995): 1878–91. https://doi.org/10.1002/j.1460-2075.1995.tb07180.x.

Werner, D., N. Gerlitz, and R. Stadler. 'A Dual Switch in Phloem Unloading during Ovule Development in Arabidopsis'. *Protoplasma* 248, no. 1 (2011): 225–35. https://doi.org/10.1007/s00709-010-0223-8.

Xie, B., X. Wang, M. Zhu, Z. Zhang, and Z. Hong. 'CalS7 Encodes a Callose Synthase Responsible for Callose Deposition in the Phloem'. *The Plant Journal : For Cell and Molecular Biology* 65, no. 1 (2011): 1–14. https://doi.org/10.1111/j.1365-313X.2010.04399.x.

Xing, S., and S. Zachgo. 'ROXY1 and ROXY2, Two Arabidopsis Glutaredoxin Genes, Are Required for Anther Development'. *Plant J* 53, no. 5 (2008): 790–801.

Yamaguchi, T., T. Hayashi, K. Nakayama, and S. Koike. 'Expression Analysis of Genes for Callose Synthases and Rho-Type Small GTP-Binding Proteins That Are Related to Callose Synthesis in Rice Anther'. *Bioscience, Biotechnology, and Biochemistry* 70, no. 3 (2006): 639–45. https://doi.org/10.1271/bbb.70.639.

Ye, C., S. Zheng, D. Jiang, J. Lu, Z. Huang, Z. Liu, H. Zhou, C. Zhuang, and J. Li. 'Initiation and Execution of Programmed Cell Death and Regulation of Reactive Oxygen Species in Plants'. *Int J Mol Sci. Nov* 30;22(23):12942 (2021). https://doi.org/10.3390/ijms222312942.

Yim, K.O., and K.J. Bradford. ‘Callose Deposition Is Responsible for Apoplastic Semipermeability of the Endosperm Envelope of Muskmelon Seeds1’. *Plant Physiology* 118, no. 1 (1998): 83–90. https://doi.org/10.1104/pp.118.1.83.

Yu, S., Q. Feng, H. Xie, S. Li, and Y. Zhang. ‘Reactive Oxygen Species Mediate Tapetal Programmed Cell Death in Tobacco and Tomato’. *BMC Plant Biology* 17 (2017).

Yuan, S., and H.H. Lin. ‘Role of Salicylic Acid in Plant Abiotic Stress’. *Z Naturforsch C* 63, no. 5–6 (2008): 313–20.

Zavaliev, R., S. Ueki, B.L. Epel, and V. Citovsky. ‘Biology of callose (β-1,3-glucan) turnover at plasmodesmata’. *Protoplasma* 248, no. 1 (2011): 117–30. https://doi.org/10.1007/s00709-010-0247-0.

Zhai, J., H. Zhang, S. Arikit, K. Huang, G.L. Nan, V. Walbot, and B.C. Meyers. ‘Spatiotemporally Dynamic, Cell-Type-Dependent Premeiotic and Meiotic PhasiRNAs in Maize Anthers’. *Proceedings of the National Academy of Sciences of the United States of America* 112, no. 10 (2015): 3146–51. https://doi.org/10.1073/pnas.1418918112.

Zhang, C., Y. Shen, D. Tang, W. Shi, D. Zhang, G. Du, Y. Zhou, G. Liang, Y. Li, and Z. Cheng. ‘The Zinc Finger Protein DCM1 Is Required for Male Meiotic Cytokinesis by Preserving Callose in Rice’. *PLOS Genetics* 14, no. 11 (2018): 1007769. https://doi.org/10.1371/journal.pgen.1007769.

Zhang, D., and Z.A. Wilson. ‘Stamen Specification and Anther Development in Rice’. *Chinese Science Bulletin* 54, no. 14 (2009): 2342–53. https://doi.org/10.1007/s11434-009-0348-3.

Zhang, F., D. Tang, Y. Shen, Z. Xue, W. Shi, L. Ren, G. Du, Y. Li, and Z. Cheng. ‘The F-Box Protein ZYGO1 Mediates Bouquet Formation to Promote Homologous Pairing, Synapsis, and Recombination in Rice Meiosis’. *The Plant Cell* 29, no. 10 (2017): 2597–2609. https://doi.org/10.1105/tpc.17.00287.

Zhao, T., L. Ren, X. Chen, H. Yu, C. Liu, Y. Shen, W. Shi, et al. ‘The OsRR24/LEPTO1 Type-B Response Regulator Is Essential for the Organization of Leptotene Chromosomes in Rice Meiosis’. *The Plant Cell* 30, no. 12 (2018): 3024–37. https://doi.org/10.1105/tpc.18.00479.

Zheng, S., J. Li, L. Ma, H. Wang, H. Zhou, E. Ni, D. Jiang, Z. Liu, and C. Zhuang. ‘OsAGO2 Controls ROS Production and the Initiation of Tapetal PCD by Epigenetically Regulating OsHXK1expression in Rice Anthers’. *Proc Natl Acad Sci U S A. Apr* 9;116(15):7549-7558

(2019). https://doi.org/10.1073/pnas.1817675116.

Preprint repository

Mimura, M., S. Ono, and K.I. Nonomura. ‘Rice MEL2 Regulates the Timing of Meiotic Transition as a Component of Cytoplasmic RNA Granules’, 2021. https://doi.org/10.1101/2021.03.24.433842